Geochemistry Geophysics Geosystems G3
AN ELECTRONIC JOURNAL OF THE EARTH SCIENCES
Published by AGU and the Geochemical Society

Article
Volume 9, Number 3
18 March 2008
Q03012, doi:10.1029/2007GC001726
ISSN: 1525-2027

Click Here for Full Article

Microstructures in Hole 1274A peridotites, ODP Leg 209, Mid-Atlantic Ridge: Tracking the fate of melts percolating in peridotite as the lithosphere is intercepted

Guenter Suhr
Institut für Geologie und Mineralogie, Universität zu Köln, Zülpicher Strasse 49b, D-50674 Cologne, Germany (guenter.suhr@uni-koeln.de)

Peter Kelemen
Lamont-Doherty Earth Observatory, Columbia University, 58 Geochemistry Building, Palisades, New York 10964, USA (peterk@ldeo.columbia.edu)

Holger Paulick
Mineralogisch-Petrologisches Institut, Universität Bonn, Poppelsdorfer Schloss, D-53115 Bonn, Germany (bolger.paulick@uni-bonn.de)

[1] We report the microstructures of harzburgites and dunites from ODP Leg 209, Hole 1274A, 15°39′N on the Mid-Atlantic Ridge. A set of features in these peridotites is so unaffected by plastic flow that it must have formed very late by magmatic processes. We believe that the microstructures record the interaction between a peridotite and a percolating melt as the thermal boundary layer was progressively intercepted. The following chronology for the microstructures is derived: Group 1, resorption of orthopyroxene (opx) associated with olivine precipitation, enhanced by a migrating melt; Group 2, conversion of opx to clinopyroxene (cpx) by a percolating melt; Group 3, precipitation of cpx and spinel as intricate intergrowth (symplectite), associated with olivine dissolution, from an interstitial melt. For these reactions the ratio of melt generated to melt consumed is progressively decreasing, as expected during progressive freezing of asthenosphere. Pristine reaction microstructures analogous to Site 1274A are also found in the Lanzo Massif (Italy) and the Little Port Complex (Canada). For all three settings we infer (1) slow spreading conditions and (2) an ancient depletion event. We thus infer that preservation of the described microstructures is favored by slow spreading and a previous depletion. Slow spreading may be required since it avoids the tectonic overprint during ductile corner flow generally inferred for fast spreading ridges. Slow spreading does not tend, however, to generate highly depleted residues because a thick lithospheric lid limits the extent of melting. Residues will thus tend to be lherzolitic, not harzburgitic. However, lherzolites have a lower permeability for mafic melts than harzburgites. In order to generate the percolation-dominated microstructures of Site 1274A, a harzburgitic host rock appears favorable. This may now explain the need for an ancient depletion event since only then can harzburgitic residues occur at the top of the mantle column during slow spreading conditions.

Components: 11,731 words, 12 figures, 3 tables.

Keywords: harzburgite; melt percolation; Mid-Atlantic Ridge; microstructures; dunite; ODP.

Index Terms: 3035 Marine Geology and Geophysics: Midocean ridge processes; 3625 Mineralogy and Petrology: Petrography, microstructures, and textures; 3036 Marine Geology and Geophysics: Ocean drilling.

Received 18 June 2007; **Revised** 22 November 2007; **Accepted** 13 December 2007; **Published** 18 March 2008.

Copyright 2008 by the American Geophysical Union

Suhr, G., P. Kelemen, and H. Paulick (2008), Microstructures in Hole 1274A peridotites, ODP Leg 209, Mid-Atlantic Ridge: Tracking the fate of melts percolating in peridotite as the lithosphere is intercepted, *Geochem. Geophys. Geosyst.*, *9*, Q03012, doi:10.1029/2007GC001726.

1. Introduction

[2] Continued research has accumulated a wealth of data pertinent to flow and melting processes under ocean ridges. Models which can explain the combined observations from geophysics [*Turcotte and Phipps Morgan*, 1992; *MELT Seismic Team*, 1998], tectonics [*Macdonald*, 2005], petrology [*Johnson et al.*, 1990; *Langmuir et al.*, 1992; *Asimov*, 1999], and ophiolites [*Nicolas and Boudier*, 1995] have reached a relatively sophisticated level. Some of the more recent models have even started to incorporate heterogeneous asthenospheric source compositions [*Seyler et al.*, 2003] and a range of options of how the lithosphere can accommodate extension during slow spreading [*Michael et al.*, 2003; *Dick et al.*, 2003; *Cannat et al.*, 2006]. Irrespective of these complexities, a basic consensus might be as follows: a variably depleted peridotite (with or without pyroxenites) is the source that starts to melt under ocean ridges. Depending on the potential temperature of the mantle this will happen in the garnet or spinel lherzolite stability field. During progressive decompression melting, melts are efficiently extracted. Melting will end as conductive cooling from above becomes important.

[3] A dramatic period for any upwelling asthenospheric peridotite is the rapid transition from adiabatic to conductive cooling conditions, i.e., the time between the onset of cooling by the overlying lithosphere and complete solidification of melt in the "lithosphere." For fast spreading conditions, it is believed that peridotites, before being converted to lithosphere, will undergo corner flow from vertical to nearly horizontal. As suggested by ophiolite studies [*Nicolas and Boudier*, 1995] this "corner flow" for ocean ridges [*Parker and Oldenburg*, 1973] occurs just below the base of gabbroic crust. In contrast, under slow spreading conditions, freezing of flow and melts presumably occurs in the steep upwelling orientation [*Nicolas*, 1989, p. 30]. In both cases, to a first order, freezing of large scale plastic flow occurs at around 1000–1100°C [*Nicolas*, 1989, p. 30]. For slow spreading, with its much thicker lithosphere, this temperature might be crossed at considerable depth [*Sleep*, 1975; *Reid and Jackson*, 1981]. For the Mid-Atlantic Ridge at 15°N, a depth for this conversion is 15–20 km and final exhumation must have occurred along more discrete, lower-temperature faults or shear zones [*Kelemen et al.*, 2004].

[4] When the conductive thermal boundary layer is encountered in the shallow mantle, a peridotite parcel will undergo rapid changes in physical conditions. For any abyssal or ophiolitic peridotite we must ask ourselves which features of the rock were formed during melting and flow in the upwelling regime and which features were imprinted on the rock during the transition from asthenospheric to lithospheric conditions. For example, are preserved ductile fabrics related to steady state upwelling conditions or formed in the transition region? Can melt percolate through a rock which is not undergoing active decompression melting? Is melt trapped at this stage in the peridotite, completely extracted, or some combination of both, with crystal fractionation followed by extraction of remaining liquid? Which reactions are steady state and which ones are affected by the thermal boundary layer? How much is deformation partitioned at the final stage?

[5] A major difference between fast and slow spreading is that during fast spreading conditions, large shear strain must be accumulated during overturn of flow from vertical to subhorizontal [*Blackman et al.*, 2002], i.e., during a period where little to no decompression melting can take place. This will not be the case for slow spreading if freezing occurs, as expected, when upwelling trajectories are nearly vertical. Therefore, generally speaking, slow spreading conditions may be better suited for study of melt transport and freezing in peridotites than fast spreading conditions because less late, accumulated strain is expected to overprint features formed during upwelling. The preservation of vertical stems in on-axis diapirs as in Oman [*Nicolas and Boudier*, 1995] may represent an important exception.

[6] In this paper, we describe the microstuctures of harzburgites and dunites from Site 1274. We also include additional evidence from peridotite massifs and ophiolites where we observe strikingly similar microstructures. Our data can best be fitted into an

overall scenario where an asthenospheric peridotite is progressively transformed into lithosphere. The main reason to invoke this general regime is that completely undeformed microstructures related to melt-migration are preserved. In a more speculative section, we explain how the excellent preservation of these microstructures may be limited to a special tectono-petrologic combination. Many of the reactions inferred from microstructural observations are comparable to those described in the recent paper by *Seyler et al.* [2007], also from Site 1274A, the results of which we cite further below.

2. Leg 209 and the 15°20′N Fracture Zone

[7] A primary goal of ODP Leg 209 was to investigate the mantle flow geometry and lithological variation in a slow spreading environment. To this end, a region with known exposure of peridotite north and south of 15°20′N at the Mid-Atlantic Ridge (the so-called Fifteen Twenty Fracture Zone) was investigated using a series of single-entry drill holes [*Kelemen et al.*, 2002]. The Fracture Zone offsets the Mid-Atlantic Ridge by 190 km. Full-spreading rates in the area are 2.5 cm/a [*Fujiwara et al.*, 2003], i.e., at the slow, but not ultra-slow (<1.2 cm/a [*Dick et al.*, 2003]) end of the spreading rate spectrum. A geochemical anomaly located just south of the Fracture Zone has yielded basalts with elevated La/Sm and $^{3}He/^{4}He$, Sr and Pb isotopes relative to MORB [*Dosso et al.*, 1993] (compilation of *Kelemen et al.* [2002, 2004]). The peridotites of the anomaly have molar Cr/(Cr + Al), or Cr# in spinel of 50 mol% and are thus elevated relative to the more regional average of 30 mol% (compilation of *Kelemen et al.* [2002, 2004]) [*Bonatti et al.*, 1992]. There is a small topographic high associated with the anomaly but no indication of an increased crustal thickness [*Fujiwara et al.*, 2003].

3. Site 1274

[8] Site 1274 is located to the west of the current ridge axis, 31 km north of the Fifteen Twenty Fracture Zone (Figure 1). Hole 1274A penetrated 156 m into the seafloor with a recovery of 35%, above average for Leg 209. The Hole is in mantle harzburgites that contain an unusually high proportion of dunite (21%) and just a few percent gabbro, while dunite was rare and gabbroic intrusions common in other peridotite sections sampled during Leg 209 [*Kelemen et al.*, 2004]. The gabbros occur mainly between 120 and 150 m, where faulting and alteration are also more abundant. Hole 1274A is the freshest peridotite Hole of Leg 209. A total of 98 samples were studied. Fifty-three were sampled on board by the Shipboard Scientific Party for the first author, and are closely spaced in and around a 3 m thick dunite between 41 and 44 mbsf. Samples described as "contact harzburgite–dunite" derive from this set. Of the other samples, twelve were taken on board by the third author, twenty three samples are shipboard polished thin sections that were borrowed from the Bremen Core Depository for microprobe-analysis, and ten are from postcruise sampling at the Bremen Core Depository by the first author.

[9] The studied samples are given in Table 1. The listed depth below seafloor in the graph is exact only for the five meter-spaced limits at which cores were retrieved. Samples could have originated at any depth between these limits unless recovery is 100%. However, "deeper" depths within the interval are for core pieces lower in the core barrel, so that relative structural order is preserved. In Figure 2, data are plotted in such a way that sample depth is spread over the core interval proportionally to the recovery rate. For example, if 25 cm of core are retrieved after drilling for 5 m below depth X, a recovery rate of 5% is indicated. A sample listed officially at a depth of X + 20 cm for this interval is thus plotted at X + 4 m depth. Modal abundances for a selected set of samples were determined by summing the area of each phase except for olivine (Table 2). Area was estimated with the help of a micrometer. The method is not very accurate for high modal abundances (i.e., orthopyroxene, "opx") but is fairly accurate for low abundances (i.e., spinel and spinel-clinopyroxene ("cpx") symplectites, see below) since none of any major grain was missed (as could easily happen during conventional point counting). The sample set consists of harzburgites, the well-defined dunite at 41 mbsf, and a zone between 70 and 90 mbsf which contains very opx-depleted harzburgites or dunites with a few percent opx (referred to as opx-depleted harzburgites even though some rocks are strictly speaking dunites). Some geochemistry is introduced here, but mainly for the purpose of supporting the microstructural arguments.

[10] An overview for the sample set is given by plotting the molar Cr/(Cr + Al) ratio, or Cr# and TiO_2 in spinels of the peridotites against depth (Figure 2 and Table 1). For harzburgites, the Cr# can act as a proxy for the total amount of melt

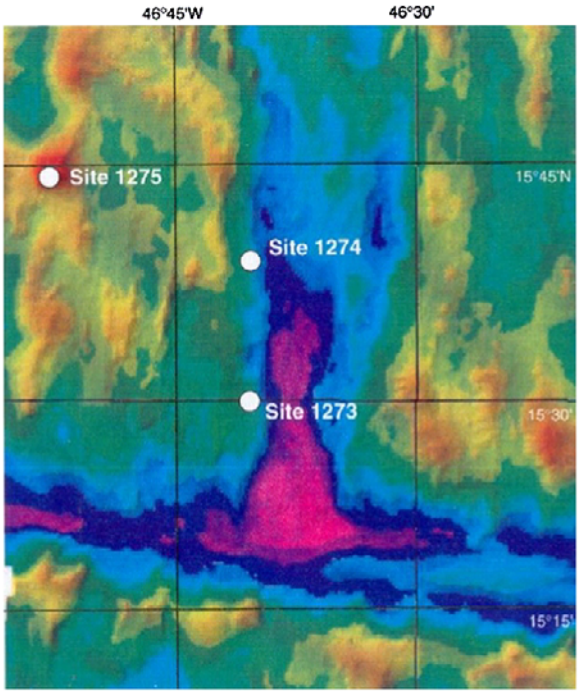

Figure 1. Location of Site 1274A north of the east-west trending Fifteen Twenty Fracture Zone [*Kelemen et al.*, 2002].

extracted [*Hellebrand et al.*, 2001]. TiO_2 in spinel gives an indication of the concentration of an alteration-resistant, moderately incompatible element. As can be seen from Figure 2, the main variation in the sample set stems from the opx-depleted harzburgites, which are essentially dunites with a few percent opx. Their Cr# of 55 mol% is above the average of 40-50 mol% for the other peridotites. Some of these opx depleted harzburgites, as well as one harzburgite in this depth range, also have a high TiO_2 in spinel (0.35%, TiO_2 in cpx up to 0.24 wt%), whereas the bulk of all other samples are below 0.1 wt%. Overall, nearly all harzburgites are geochemically more akin to the anomalous peridotites known from south of the Fifteen Twenty Fracture Zone than to the more regional average with a Cr# of ~30 mol% occurring between 0° and 25°N along the Mid-Atlantic Ridge as given by *Bonatti et al.* [1992]. In Figure 3 and Table 3, average trace element contents in cpx are given for the three main lithological groups. The harzburgite data are compatible with the concentrations given by *Seyler et al.* [2007]. Compared to the harzburgites, dunites and opx-depleted harzburgites have elevated HREE and Ti, but are still completely unlike any trace element pattern which could be in equilibrium with MORB. The extreme depletion in middle REE, as observed in dunites and harzburgites, is the reason for postulating initiation of melting in the garnet stability field [*Seyler et al.*, 2007]. This middle REE depletion is less pronounced in the opx-depleted harzburgites which may thus have a different origin.

[11] For a more detailed evaluation of the geochemistry, the reader is referred to the modeling of *Seyler et al.* [2007]. According to these authors, the peridotites represent residues from a combination of ~10 wt% melting in the garnet stability field followed by another 15 wt% melting in the spinel stability field. This was probably followed by lower pressure melt percolation in order to account for the variable proportion of orthopyroxene. Some of the melting is probably ancient and unrelated to the current convective regime, as shown by *Harvey et al.* [2006] on the basis of Os-isotopes.

4. General Microstructure Observations

[12] In all peridotites, including the dunitic rocks, several characteristic microstructural features are observed. We first give a more general overview, then discuss the origin of the most characteristic features, providing additional observations and relevant documentation.

[13] Olivines are coarse-grained and lack obvious solid-state deformation microstructures on the scale of a thin section. The presence or absence of a crystallographic preferred orientation could not be verified. In some dunites, aligned spinel tablets (exsolutions) occur in olivine. Overall, the olivine microstructures are typical for low-stress, high-temperature conditions (i.e., coarse granular). A mylonitic (high-stress, low-T) overprint was only found in samples 1274A-12R1-13 and -18.

[14] Orthopyroxene (opx) crystals tend to form aggregates of grains as is typical in mantle peridotites (Figures 4a and 4b). The coarsest of these clusters are up to 1 cm in diameter. Outlines of single grains range from convex to concave. A convex outward shape with locally perfect rounding is most pronounced where opx is rimmed by cpx. Such opx grains rimmed by cpx are typically isolated or consist of a maximum of two clustering grains. In about every third harzburgite thin section studied, an opx cluster is associated with coarse, massive spinel or with a coarse vermicular spinel (Figure 4a). The more massive the spinel, the more it tends to be located within the center of an opx-cluster (Figure 4b). Opx with the same character-

Table 1. Sample Sources and Their Averaged Spinel Chemistry

Designator	Rock Type	Source	N[a]	SiO_2	TiO_2	Al_2O_3	Cr_2O_3	FeO	MgO	MnO	NiO	CaO	Total	Cr#	Mg#	Fe_2O_3[b]
1274_01R1_2	hzbg	Shipboard	4	0.35	0.049	37.6	32.8	12.8	16.9	0.13	0.18	0.00	100.9	36.9	70.6	0.20
1274_01R1_4	hzbg	Suhr 2nd	7	0.02	0.045	39.1	33.0	12.6	17.5	0.18	0.17	0.01	102.6	36.1	72.1	0.62
1274_03R1_9C	hzbg	Paulick	7	0.02	0.046	33.5	38.0	13.0	16.8	0.19	0.15	0.00	101.7	43.2	71.4	1.14
1274_03R1_9B	hzbg	Shipboard	6	0.02	0.036	32.3	38.5	14.0	15.6	0.18	0.10	0.00	100.7	44.4	67.8	0.86
1274_04R1_3	hzbg	Shipboard	11	0.02	0.057	30.4	40.7	13.6	15.8	0.20	0.14	0.01	101.0	47.4	69.0	1.09
1274_05R2_10B	hzbg	Shipboard	6	0.01	0.051	34.9	36.0	13.6	15.9	0.20	0.15	0.00	100.9	40.9	68.4	0.54
1274_05R2_1B	hzbg	Shipboard	7	0.03	0.046	32.2	39.0	13.1	15.7	0.17	0.13	0.01	100.5	44.9	68.9	0.49
1274_06R2_1A-26	hzbg	Shipboard	6	0.02	0.042	33.1	38.0	13.8	15.5	0.20	0.11	0.00	100.9	43.5	67.3	0.38
1274_06R2_1A-63	hzbg	Shipboard	3	0.64	0.038	31.0	39.0	14.4	15.2	0.21	0.14	0.23	100.9	45.8	65.4	0.15
1274_06R2_4	hzbg	Paulick	5	0.02	0.038	30.8	40.7	14.3	15.9	0.23	0.08	0.00	102.1	47.0	68.6	1.42
1274_06R3_1B	hzbg	Shipboard	5	0.01	0.033	30.2	40.6	14.3	15.0	0.20	0.11	0.02	100.5	47.4	66.0	0.68
1274_07R1_5	hzbg	Shipboard	5	0.01	0.032	30.5	39.7	15.5	14.7	0.23	0.10	0.00	100.8	46.6	64.7	1.39
1274_07R1_7A	hzbg	Shipboard	8	0.02	0.038	30.0	41.7	13.9	15.6	0.20	0.14	0.02	101.7	48.3	67.9	0.86
1274-07R2_1	hzbg	Suhr	12	0.02	0.042	29.3	41.8	13.9	15.8	0.19	0.13	0.02	101.3	48.9	68.8	1.36
1274-07R2_2a	hzbg	Suhr	5	0.02	0.029	30.0	41.1	15.2	15.2	0.23	0.12	0.02	101.9	47.9	66.4	1.60
1274-07R2_2b	hzbg	Suhr	7	0.02	0.017	31.3	39.5	14.1	15.4	0.21	0.14	0.04	100.8	45.9	67.3	0.86
1274-07R2_3	hzbg	Suhr	4	0.02	0.028	29.7	41.2	14.3	15.6	0.23	0.12	0.03	101.2	48.2	68.3	1.49
1274-08R1_1	hzbg, px rich	Suhr	5	0.02	0.039	30.4	41.9	14.1	15.6	0.22	0.16	0.00	102.5	48.0	67.5	0.72
1274-08R1_2	hzbg, cpx rich	Suhr	10	0.03	0.043	29.1	42.0	13.8	15.9	0.20	0.13	0.00	101.2	49.2	69.5	1.44
1274-08R1_3	hzbg	Suhr	7	0.02	0.045	28.4	42.5	14.9	15.4	0.21	0.13	0.00	101.6	50.1	67.4	1.84
1274-08R1_4	hzbg, px rich	Suhr	6	0.02	0.031	29.6	41.0	14.9	15.0	0.22	0.11	0.03	101.0	48.2	66.0	1.27
1274-08R1_5	du/hz trans	Suhr	2	0.02	0.058	28.0	40.3	17.1	14.8	0.23	0.18	0.01	100.8	49.1	65.7	3.66
1274-08R1_6	hz, bitopx depl	Suhr	6	0.02	0.037	31.4	38.2	15.3	15.3	0.24	0.15	0.03	100.8	44.9	67.0	2.07
1274-08R1_7	hzbg	Suhr	6	0.01	0.052	28.5	42.3	14.2	15.9	0.20	0.13	0.00	101.4	49.9	69.6	2.03
1274-08R1_8	hzbg	Suhr	4	0.02	0.031	30.3	39.2	15.7	14.9	0.20	0.14	0.02	100.5	46.5	65.6	1.99
1274-08R1_9	du	Suhr	6	0.03	0.093	29.1	41.3	14.2	16.3	0.21	0.12	0.01	101.2	48.8	70.7	2.41
1274-08R1_10	hz-du trans	Suhr	5	0.02	0.044	27.1	41.3	17.0	13.9	0.27	0.12	0.02	99.8	50.6	63.0	2.63
1274-08R1_11	du	Suhr	8	0.03	0.091	30.0	40.7	14.2	16.2	0.23	0.13	0.00	101.5	47.7	70.1	2.09
1274-08R1_12.2	du	Suhr	3	0.05	0.084	31.7	38.4	14.2	16.0	0.19	0.10	0.00	100.8	44.8	69.4	1.78
1274-08R1_13	du	Suhr	9	0.26	0.084	29.5	41.3	14.6	16.0	0.23	0.13	0.00	102.2	48.5	68.8	1.89
1274-08R1_14	du	Suhr	7	0.02	0.071	27.6	41.9	15.7	14.8	0.24	0.09	0.00	100.4	50.4	65.8	2.20
1274-08R1_15c3	du	Suhr	9	0.03	0.078	28.8	41.6	15.2	15.6	0.19	0.14	0.00	101.7	49.2	68.0	2.39
1274-08R1_15.5	du	Suhr	6	0.03	0.085	29.8	40.4	14.7	16.0	0.20	0.13	0.00	101.3	47.6	69.7	2.48
1274-08R1_16	du	Suhr	4	0.04	0.093	29.2	41.9	14.5	16.4	0.20	0.13	0.00	102.5	49.1	70.4	2.53
1274-08R1_17	du	Suhr	7	0.03	0.079	28.2	43.2	15.1	15.2	0.20	0.08	0.01	102.1	50.7	66.3	1.51
1274-08R1_18	du	Suhr	7	0.03	0.083	27.9	42.0	14.3	15.9	0.21	0.16	0.00	100.6	50.3	70.1	2.42
1274-08R1_19	du	Suhr	10	0.03	0.068	29.3	41.5	15.0	15.7	0.21	0.13	0.02	101.9	48.7	68.3	2.18
1274-08R1_20	du	Suhr	5	0.03	0.086	27.6	42.8	15.0	15.7	0.21	0.14	0.00	101.6	50.9	68.9	2.62
1274-08R2_1	du	Suhr	4	0.03	0.060	28.8	41.1	15.0	15.2	0.21	0.15	0.04	100.7	48.9	67.2	1.96
1274-08R2_2	du	Suhr	8	0.03	0.078	28.3	42.3	14.6	15.9	0.23	0.15	0.00	101.6	50.0	69.6	2.41
1274-08R2_3	du	Suhr	7	0.03	0.074	28.3	41.8	14.7	15.8	0.20	0.13	0.00	101.0	49.7	69.4	2.49
1274-08R2_4	du	Suhr	12	0.04	0.081	28.9	42.4	14.6	16.0	0.22	0.13	0.00	102.4	49.6	69.3	2.15
1274-08R2_5	du	Suhr	6	0.02	0.068	30.0	40.0	14.9	15.4	0.19	0.13	0.00	100.7	47.2	67.5	1.87
1274-08R2_6	du	Suhr	7	0.02	0.067	27.5	42.0	16.8	14.8	0.24	0.09	0.00	101.5	50.6	65.1	3.02
1274-08R2_8	du?	Suhr	5	0.03	0.086	30.1	40.9	14.2	15.9	0.19	0.12	0.00	101.6	47.6	69.0	1.67
1274-08R2_9	du	Suhr	4	0.04	0.078	30.4	39.8	15.1	15.6	0.18	0.13	0.03	101.3	46.7	67.7	2.06
1274-08R2_10	hzbg	Suhr	3	0.03	0.056	29.0	42.1	13.4	15.6	0.19	0.11	0.00	100.5	49.4	68.8	0.87
1274-08R2_11	hzbg	Suhr	4	0.03	0.051	29.1	41.3	13.3	15.6	0.24	0.13	0.00	99.7	48.7	68.9	0.89
1274-08R2_12	hzbg	Suhr	7	0.02	0.043	29.7	40.8	13.5	15.2	0.21	0.12	0.02	99.6	47.9	67.5	0.46
1274-08R2_13	hzbg	Suhr	4	0.02	0.064	30.6	40.3	13.5	16.0	0.19	0.11	0.00	100.7	46.9	69.7	1.18
1274-08R2_14	du	Suhr	4	0.02	0.095	32.0	38.5	13.6	16.6	0.20	0.13	0.00	101.2	44.7	71.5	1.99
1274-08R2_15	hzbg	Suhr	7	0.06	0.054	33.0	38.5	13.9	15.9	0.19	0.13	0.00	101.7	43.9	68.1	0.64
1274-08R2_17	hzbg	Suhr	10	0.02	0.050	32.6	38.0	13.2	16.1	0.17	0.11	0.01	100.3	43.8	69.9	0.95
1274-08R2_18	hzbg	Suhr	8	0.01	0.047	31.8	39.3	13.3	16.2	0.19	0.15	0.02	101.1	45.3	70.2	1.17
1274-08R2_19	hzbg	Suhr	6	0.02	0.047	33.0	37.0	13.7	15.3	0.19	0.12	0.00	99.4	42.9	67.0	0.32
1274-08R2_20	hzbg	Suhr	4	0.01	0.054	34.1	36.0	14.0	15.6	0.18	0.13	0.00	100.0	41.4	67.6	0.75
1274-08R2_21	hzbg	Suhr	3	0.02	0.050	35.3	35.7	13.7	16.3	0.20	0.14	0.00	101.4	40.4	69.2	0.94
1274-09R1_1	hzbg	Suhr	6	0.02	0.051	32.2	40.0	13.7	15.9	0.17	0.11	0.02	102.1	45.4	68.0	0.44
1274-09R1_2	hzbg	Suhr	3	0.01	0.049	33.7	36.9	14.1	15.9	0.18	0.12	0.03	101.0	42.4	68.4	1.13
1274-09R1_3	hzbg	Suhr	4	0.03	0.035	30.5	40.3	14.5	15.6	0.21	0.12	0.01	101.2	47.0	67.8	1.48
1274-09R1_4	hzbg	Suhr	7	0.03	0.059	33.8	38.2	14.0	16.2	0.18	0.14	0.01	102.6	43.2	68.6	0.87
1274-09R1_5	hzbg	Suhr	3	0.02	0.042	34.6	36.0	13.7	16.3	0.17	0.16	0.00	101.0	41.1	69.6	1.13

Table 1. (continued)

Designator	Rock Type	Source	N[a]	SiO_2	TiO_2	Al_2O_3	Cr_2O_3	FeO	MgO	MnO	NiO	CaO	Total	Cr#	Mg#	Fe_2O_3[b]
1274-09R1_6	hzbg	Suhr	3	0.03	0.058	32.2	39.1	14.3	15.9	0.18	0.10	0.02	101.8	44.9	68.1	1.16
1274-09R1_7	hzbg	Suhr	7	0.03	0.053	33.4	37.9	14.1	16.0	0.21	0.15	0.00	101.9	43.3	68.3	0.99
1274-09R1_8	hzbg	Suhr	8	0.02	0.055	35.0	36.1	13.7	16.4	0.18	0.15	0.01	101.6	40.9	69.6	1.07
1274-09R1_9	hzbg	Suhr	3	0.03	0.059	34.1	36.8	13.5	16.6	0.18	0.12	0.01	101.3	42.0	70.7	1.35
1274-10R1_2	du, 1 opx	Paulick	5	0.10	0.052	29.0	41.0	15.3	15.2	0.23	0.10	0.00	100.9	48.6	66.5	1.93
1274-11R1_12B	hzbg	Shipboard	6	0.02	0.049	30.2	41.9	13.5	16.4	0.23	0.16	0.01	102.4	48.2	70.5	1.38
1274-12R1_13	hzbg	Shipboard	5	0.02	0.067	30.9	40.5	13.9	16.0	0.21	0.11	0.00	101.7	46.8	69.1	1.25
1274-12R1_18	hzbg	Paulick	3	0.09	0.074	32.2	40.0	13.8	15.9	0.24	0.08	0.00	102.4	45.5	67.9	0.44
1274-13R1_1	hzbg	Shipboard	7	0.02	0.067	31.3	40.3	13.3	16.3	0.22	0.12	0.00	101.6	46.3	70.2	1.09
1274_13R1_04	hzbg	Suhr 2nd	7	0.02	0.057	31.4	41.2	13.7	16.4	0.23	0.12	0.00	103.1	46.8	69.7	1.13
1274-14R1_5	hzbg	Paulick	5	0.02	0.138	31.6	40.0	14.1	16.2	0.22	0.15	0.00	102.5	45.9	69.3	1.43
1274-14R1_8C	hzbg	Shipboard	5	0.04	0.124	31.3	39.6	14.2	16.0	0.20	0.12	0.01	101.6	45.9	68.8	1.48
1274_14R1_11	hzbg	Suhr 2nd	6	0.01	0.131	32.8	38.5	14.7	16.0	0.20	0.12	0.02	102.5	44.0	68.3	1.56
1274-15R1_4A	du	Shipboard	3	0.02	0.120	24.6	45.9	16.0	15.0	0.21	0.14	0.00	102.0	55.6	66.8	2.94
1274_15R1_09	depl hzbg	Suhr 2nd	5	0.05	0.230	25.2	46.7	15.2	15.1	0.23	0.09	0.00	102.7	55.4	66.2	1.61
1274-15R1_15A	depl hzbg	Paulick	4	0.02	0.151	24.1	45.9	18.6	12.4	0.26	0.10	0.00	101.7	56.1	56.2	1.59
1274-15R1_15A	depl hzbg	Shipboard	10	0.01	0.168	24.7	45.7	15.5	14.2	0.23	0.09	0.01	100.7	55.4	64.1	1.45
1274_15R2_01	depl hzbg	Suhr 2nd	5	0.10	0.156	25.6	46.1	15.2	15.0	0.21	0.11	0.00	102.5	54.7	65.9	1.51
1274-15R2_05	hzbg	Paulick	4	0.02	0.153	24.6	47.1	15.3	14.8	0.20	0.10	0.00	102.3	56.2	65.6	1.63
1274_15R2_11	depl hzbg	Suhr 2nd	5	0.03	0.145	25.7	46.4	15.2	15.2	0.21	0.08	0.00	102.9	54.8	66.5	1.67
1274_16R1_04	depl hzbg	Suhr 2nd	4	0.02	0.277	27.7	44.4	15.0	15.4	0.20	0.12	0.00	103.1	51.8	66.4	1.22
1274-16R1_07	depl hzbg	Paulick	5	0.03	0.259	27.8	43.6	14.3	15.2	0.21	0.10	0.00	101.5	51.3	66.5	0.76
1274_16R2_01B	depl hzbg	Suhr 2nd	5	0.03	0.346	24.7	46.4	14.4	15.3	0.21	0.13	0.00	101.6	55.8	67.7	1.50
1274-16R2_01B	depl hzbg	Shipboard	4	0.03	0.336	25.4	46.6	14.5	15.6	0.20	0.13	0.00	102.7	55.2	68.1	1.58
1274_16R2_08	depl hzbg	Suhr 2nd	5	0.08	0.300	24.7	47.2	14.7	15.2	0.22	0.12	0.00	102.4	56.2	66.6	1.23
1274-17R1_6A	depl hzbg	Shipboard	9	0.02	0.191	25.4	46.2	14.7	14.8	0.20	0.11	0.00	101.6	54.9	65.7	0.99
1274_17R1_08	depl hzbg	Suhr 2nd	4	0.02	0.116	26.7	43.0	17.5	14.3	0.27	0.11	0.00	101.9	52.0	63.1	2.92
1274-17R1_21	hzbg	Paulick	5	0.02	0.047	28.7	43.1	14.3	15.8	0.24	0.11	0.02	102.4	50.2	68.8	1.67
1274-17R2_1B	hzbg	Shipboard	8	0.06	0.080	34.1	37.1	13.0	16.9	0.19	0.16	0.00	101.6	42.3	71.8	1.26
1274-18R1_15	hzbg	Paulick	7	0.02	0.060	32.7	39.3	13.6	16.6	0.22	0.17	0.01	102.7	44.6	70.6	1.36
1274-18R1_19A	hzbg	Shipboard	8	0.03	0.063	31.9	39.7	13.5	16.3	0.22	0.13	0.01	101.9	45.5	70.1	1.28
1274-20R1_23	dunite	Paulick	4	0.02	0.141	28.9	37.9	19.1	15.0	0.21	0.14	0.00	101.4	46.8	65.6	5.61
1274-20R1_26A	dunite	Shipboard	7	0.03	0.196	25.8	44.6	15.6	15.3	0.23	0.10	0.00	101.7	53.7	67.2	2.59
1274-22R1_4	hzbg	Paulick	4	0.02	0.038	27.4	44.2	13.9	15.9	0.24	0.10	0.00	101.8	52.0	69.6	1.75
1274-27R1_8A	hzbg	Shipboard	9	0.02	0.107	30.2	41.2	14.0	15.9	0.20	0.10	0.01	101.7	47.8	68.8	1.25
1274-27R2_2	hzbg	Paulick	7	0.02	0.078	31.1	40.8	13.9	16.1	0.20	0.13	0.00	102.4	46.8	69.1	1.17

[a] N, number of single analyses in average.
[b] Fe2O3 calculated on assumption of stoichiometric spinel.

istics occurs in the opx-depleted samples between 75 and 90 mbsf. Modal abundance of opx in harzburgites is variable but generally low (10–15 vol%, Figure 5). The mean abundance from our measurements is lower than that of *Seyler et al.* [2007], who determined 20.6 vol% average modal opx.

[15] Clinopyroxene (cpx) occurs as thin, partial to complete rim on opx, as mentioned above (Figures 6a–6d and 7b). Typically, the rims are ~10 μm thick, but exceptionally they may be just 1–2 μm or up to 100 μm. In samples 1274A-7R2-1 to 8R1-4 cpx also occurs as larger grains up to 1 mm, but typically with tips protruding into the olivine matrix (Figure 6f). Large cpx grains associated with opx clusters (typical for lherzolites) were not observed. Cpx also occurs as interstitial grain within the olivine matrix. Thus, on the basis of shape of cpx or association with other phases, there are no grains of cpx which can be classified as porphyroclastic (i.e., residual), as also inferred by *Seyler et al.* [2007]. The break in the opx content at 40.3 m as reported by the shipboard party [*Kelemen et al.*, 2004] is marked in our samples by the disappearance of larger cpx grains. Particularly in some dunites, interstitial cpx grains are so extensive that they can be classified as poikilitic. However, other dunite thin sections are entirely cpx-free. Cpx distribution in dunites is thus heterogeneous. Cpx in dunites locally also occurs as rims on spinel and as massive grains. Cpx inclusions are common in spinel in dunite. A further generation of cpx occurs intricately intergrown with spinel, both in harzburgites and dunites (symplectites, see below). Where different cpx textural associations occur within in a single slide (i.e., massive cpx grains, cpx rims, interstitial,

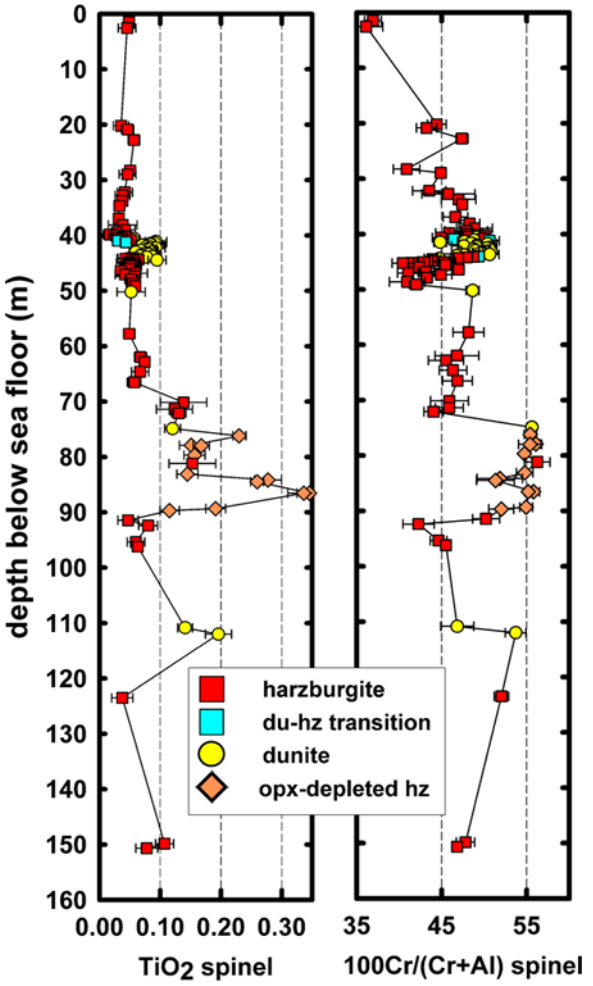

Figure 2. Downhole mineral chemical variation of spinel in Hole 1274A. Note special character of the opx-depleted harzburgites at 75–90 mbsf.

symplectites) they could not be discriminated in terms of major or trace element chemistry. The mode of cpx is 0–0.5 vol% with no correlation to any lithology (Figure 5c).

[16] Spinel occurs as coarse-grained intergrowths with opx or massive grain associated with opx (see above), as symplectite (see below) and (in dunites and opx-depleted harzburgites) as massive, isolated grains. A shape-preferred orientation is not apparent. In some samples, spinel occurs solely as part of the symplectitic grains. Where spinels are present as larger, massive grains, the sample is modally enriched in spinel up to 1 vol-%, in dunites up to 4.5% (Figure 5b). Apparently, modal homogeneity is not present on a thin section scale, particularly in dunites. Spinel in dunite is commonly associated with cpx.

[17] An intricate, texturally varied intergrowth of spinel and cpx occurs in all peridotite samples studied. It is referred to as "symplectite" and is treated as a generation distinct from monophase cpx or spinel (Figures 8 and 9). Its mode ranges typically up to 0.4%, exceptionally reaches 0.8%, averaging 0.2 vol% (Figure 5a). The highest abundance tends to occur at the contact of dunite to harzburgite, as well as locally within the dunites. There are cases when morphological transitions occur to a similar intergrowth of opx with spinel, which then typically contains minor cpx (Figures 4c–4e). Specifically, the cpx-spinel symplectites occur (1) along the margins of opx grains, commonly at the tip of elongated opx grains; (2) as isolated grains in the olivine matrix; and (3) as rims on clinopyroxene.

[18] Typically, symplectites are <400 μm in maximum extent. Exceptionally, they reach 1.5 mm length as in 6R2-1A and dunite 8R1-10. The modal proportion of clinopyroxene to spinel varies mainly between 3:1 to 2:1 (by image analysis of backscatter electron images, Figure 5d). The spacing of the wormy spinels ranges from 10 μm upward. The interface symplectite/olivine may be extremely ragged whereas the contact symplectite to cpx or opx tends to be smooth.

5. Preferred Interpretations

[19] Harzburgite microstructures from Hole 1274A, Leg 209, have recently been documented by *Seyler et al.* [2007]. Our interpretation agrees to a first order with *Seyler et al.* [2007], even though our arguments to arrive at the interpretations are somewhat different, perhaps also more specific. A reason might be that our database includes dunites and opx-depleted harzburgites. These are presumably the rocks most affected by reaction with migrating melt, and our interpretation, like that by *Seyler et al.* [2007], strongly emphasizes the importance of reaction with percolating melts to generate the microstructures. Our sample-base for lherzolitic samples with large cpx grains is small, unlike that of *Seyler et al.* [2007], so that we cannot add much to understanding the origin of these rocks. Since our paper is mainly a microstructural paper, we present a classification and attempt a more comprehensive synthesis of textural observations, also within a geodynamic context. *Seyler et al.* [2007], however, incorporate trace elements and base metal sulfides in their synthesis.

Table 2. Modes as Determined by Counting Areas of Phases Except for Olivine[a]

	Rock Type	Symplectite	Cpx	Spinel	Opx	Olivine by Difference
Opx-dunites						
15R1-9	depl hz	0.0024	0.0000	0.0060	0.01	0.98
15R1-15A(AP92)	depl hz	0.0022	0.0014	0.0061	0.05	0.94
15R2-1	depl hz	0.0023	0.0027	0.0050	0.05	0.94
15R2-11	depl hz	0.0016	too altered	0.0038	0.06	0.94
16R1-7 (AP94)	depl hz	0.0003	traces	0.0003	0.05	0.95
16R2-1B	depl hz	0.0000	too altered	0.0000	0.05	0.95
16R1-4	depl hz	0.0006	too altered	0.0004	0.03	0.97
17R1-8	depl hz	0.0003	all altered	0.0003	0.02	0.98
Avg mode opx-dunite		**0.001**		**0.003**	**0.040**	
Dunites						
8R1-9	du	0.0011	0.0000	0.0000	0.00	1.00
8R1-11	du	0.0000	0.0000	0.0045	0.00	1.00
8R1-13	du	0.0012	0.0000	0.0045	0.00	0.99
8R1-14	du	0.0003	0.0003	0.0001	0.00	1.00
8R1-15	du	0.0033	0.0006	0.0143	0.00	0.98
8R1-17	du	0.0000	0.0041	0.0003	0.00	1.00
8R1-18	du	0.0016	0.0000	0.0465	0.00	0.95
8R1-19	du	0.0052	0.0105	0.0015	0.00	0.98
8R2-2	du	0.0042	0.0000	0.0389	0.00	0.96
8R2-3	du	0.0020	0.0000	0.0118	0.00	0.99
8R2-4	du	0.0071	0.0001	0.0176	0.00	0.98
8R2-8	du	too alt? None	too alt? None	0.0017	0.00	1.00
Avg mode dunite		**0.002**	**0.001**	**0.013**		
Harzburgites						
1R1-4	hz	0.0009	0.0005	0.0042	0.13	0.86
7R2-1	hz	0.0023	0.0178	0.0108	0.14	0.83
7R2-2B	hz	0.0038	0.0021	0.0004	0.11	0.88
8R1-1	hz	0.0015	0.0009	0.0033	0.16	0.84
8R1-2	hz	0.0015	0.0250	0.0055	0.11	0.86
8R1-4	hz	0.0022	0.0034	0.0009	0.17	0.82
8R1-6	hz	0.0019	0.0018	0.0001	0.11	0.89
8R2-11	hz	0.0014	0.0023	0.0009	0.14	0.86
8R2-15	hz	0.0018	0.0006	0.0022	0.13	0.87
8R2-17	hz	0.0031	0.0005	0.0051	0.13	0.86
8R2-19	hz	0.0010	0.0001	0.0008	0.14	0.86
9R1-1	hz	0.0051	0.0015	0.0003	0.08	0.91
9R1-4	hz	0.0012	0.0000	0.0026	0.15	0.85
9R1-8	hz	0.0022	0.0006	0.0006	0.15	0.85
12R1-18 (AP89)	hz	0.0014	0.0015	0.0009	0.10	0.90
14R1-5 (AP091)	hz	0.0026	0.0002	0.0042	0.08	0.91
14R1-11	hz	0.0028	0.0008	0.0006	0.12	0.87
15R2-05 (AP93)	hz	0.0021	0.0024	0.0010	0.18	0.81
16R2-8	hz	0.0002		0.0029	0.08	0.91
27R2-2 (AP103)	hz	0.0024	0.0003	0.0010	0.10	0.89
Avg mode harzburgite		**0.002**	**0.003**	**0.002**	**0.13**	**0.87**
Std mode harzburgite		**0.001**	**0.007**	**0.003**	**0.03**	
Contacts						
8R1-8	contact hz-du	0.0077	0.0010	0.0000	0.16	0.83
8R1-10	contact hz-du	0.0038	0.0035	0.0000	0.07	0.92
8R2-10	contact hz-du	0.0038	0.0017	0.0011	0.16	0.84

[a] Abbreviations: avg, average; std, one standard deviation.

5.1. Group 1: Opx-Spinel Association in Clusters (Figures 4a and 4b)

[20] The bulk of all peridotites are chemically highly depleted and have a very low mode of cpx and even opx compared to a fertile peridotite. Typical melting reactions in the spinel peridotite stability field have been investigated extensively by experiment. In terms of modal balance during melting at lower pressures, they are cpx $\gg$ opx $>$ 0 $>$

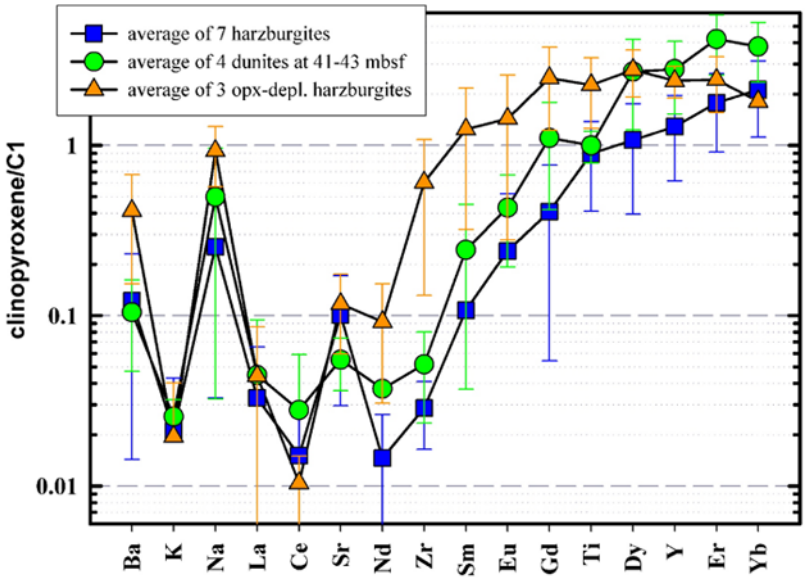

Figure 3. Averaged trace element patterns in samples from Site 1274A as determined by secondary ion mass spectrometry on cpx grains using conditions and methods as given by *Hellebrand et al.* [2002]. Error bars are one sigma values of the averages of each sample, each sample having typically two to three analyses.

olivine (summary by *Walter* [2003]) where consumption is positive and production is negative. Spinels become progressively more chromiferous [*Jaques and Green*, 1980]. Thus

$$\text{X opx} + \text{Y cpx} + \text{Z Al} - \text{spinel} = \text{A olivine} + \text{B Cr} - \text{spinel} + \text{C melt} \quad (1a)$$

where X is less than Y, A and C vary substantially with pressure, and Z and B depend critically on bulk composition.

[21] To a first order, the observed low proportions of cpx and opx, compared to their proportions in the MORB source [e.g., *Workman and Hart*, 2005], and the occurrence of Cr-rich spinel, are thus compatible with the above reaction. In addition, adiabatic reaction between pyroxenes and ascending melt, produced deeper in the mantle, produces a very similar outcome [e.g., *Kelemen et al.*, 1990; *Asimov*, 1999], with dissolution of both pyroxenes, production of olivine + Cr-spinel, and an increase in the melt mass. This reasoning suggests that partial

Table 3. Averaged Cpx Trace Element Concentrations in Cpx[a]

	Avg Hzbg	Std Hzbg	Avg Du	Std Du	Avg Depl. Hz	Std Depl. Hz
Na	1272	1108	2488	2325	4646	1786
K	11.5	11.9	13.9	3.5	10.6	11.4
Ti	398	216	445	94	1006	445
Cr	7546	2727	7857	858	8493	805
Sr	0.73	0.51	0.40	0.14	0.85	0.42
Y	2.0	1.1	4.4	2.0	3.8	0.8
Zr	0.11	0.05	0.20	0.11	2.35	1.84
Ba	0.30	0.26	0.25	0.14	1.00	0.62
La	0.008	0.008	0.011	0.012	0.010	0.010
Ce	0.009	0.008	0.017	0.019	0.006	0.003
Nd	0.008	0.005	0.023	0.024	0.043	0.029
Sm	0.019	0.020	0.037	0.032	0.190	0.141
Eu	0.014	0.016	0.025	0.014	0.083	0.067
Gd	0.084	0.073	0.23	0.14	0.51	0.26
Dy	0.27	0.17	0.69	0.38	0.70	0.22
Er	0.29	0.14	0.70	0.27	0.40	0.14
Yb	0.36	0.17	0.65	0.25	0.31	0.01

[a] Concentrations in cpx are in ppm. Harzburgite, 7 samples; dunite, 4 samples; opx-depleted harzburgite, 3 samples. Abbreviations: avg, average; std, one standard deviation.

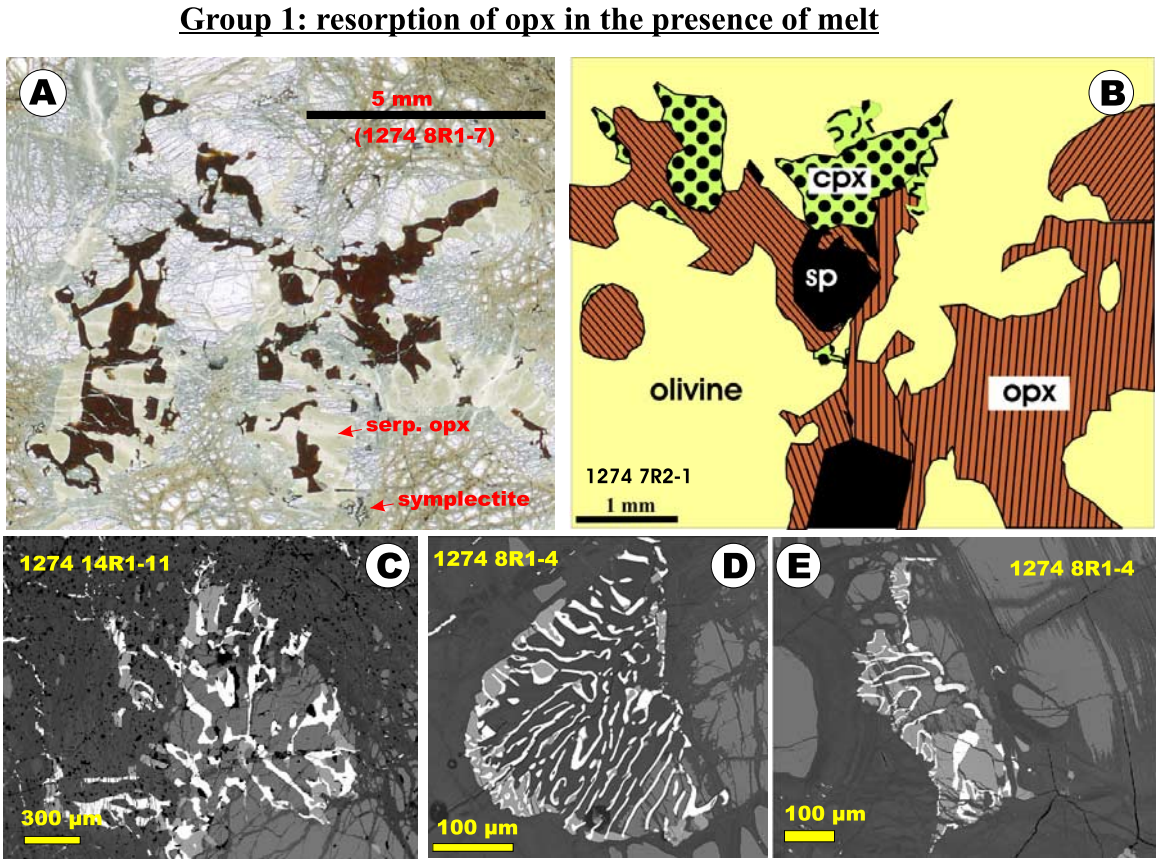

Figure 4. (a) Optical image of a large opx-cluster coarsely intergrown with spinel. Opx is serpentinized. One symplectite is present at bottom center. (b) Drawing from microscope picture of very irregular-shaped opx cluster with massive spinels in the center of the grain plus some cpx; Figure 4b might be an annealed form of Figure 4a. (c–e) Backscattered electron images of spinel-opx symplectites transitional to a marginal cpx-spinel symplectite. All occurrences are located on an opx tip (not visible on this scale).

melting may have been the major time-integrated process which produced the residual bulk compositions of these rocks. However, besides the proportion and composition of minerals, is there any microstructural memory of this process?

[22] The above reaction generates harzburgite from lherzolite. Chromium is a neutral to compatible element during melting [e.g., *Liang and Elthon*, 1990], i.e., in combination with melt/solid ratios $\ll 1$ during melting and melt percolation (“low porosity”), the element will be relatively immobile. Why, then, is Cr-spinel unevenly distributed, particularly in dunites (Figure 5b)? It is suggested that during melting, Cr had a limited mobility (in the order of 10 cm), probably via transport or diffusion in the melt over a short distance before precipitating around existing spinel. This could explain the highly variable abundance of spinel in thin sections. The occurrence of spinel as massive grains as opposed to coarse intergrowths with opx is thought to be the result of annealing of the coarser texture at high temperatures (under hypersolidus conditions) to form the massive grains. Why spinel would preferentially be located in the center of opx-grains (Figures 4a and 4b) is not clear.

[23] Opx in these coarse clusters commonly has concave boundaries toward the olivine matrix (Figure 4b), in contrast to convex boundaries of opx rimmed by cpx (discussed below). It appears that the concave boundaries facing olivine should reflect a feedback mechanism whereby melting or dissolution of opx generated conditions which favored even more resorption of opx. Perhaps such a feedback could be caused by an infiltrating melt. If an infiltrating melt caused additional melt to form, porosity would be generated at the site of initial melting and this porosity could feed back into a hydraulic gradient channeling even more melt into the site of melting (i.e., the fluid dynamic concept of the reactive infiltration instability

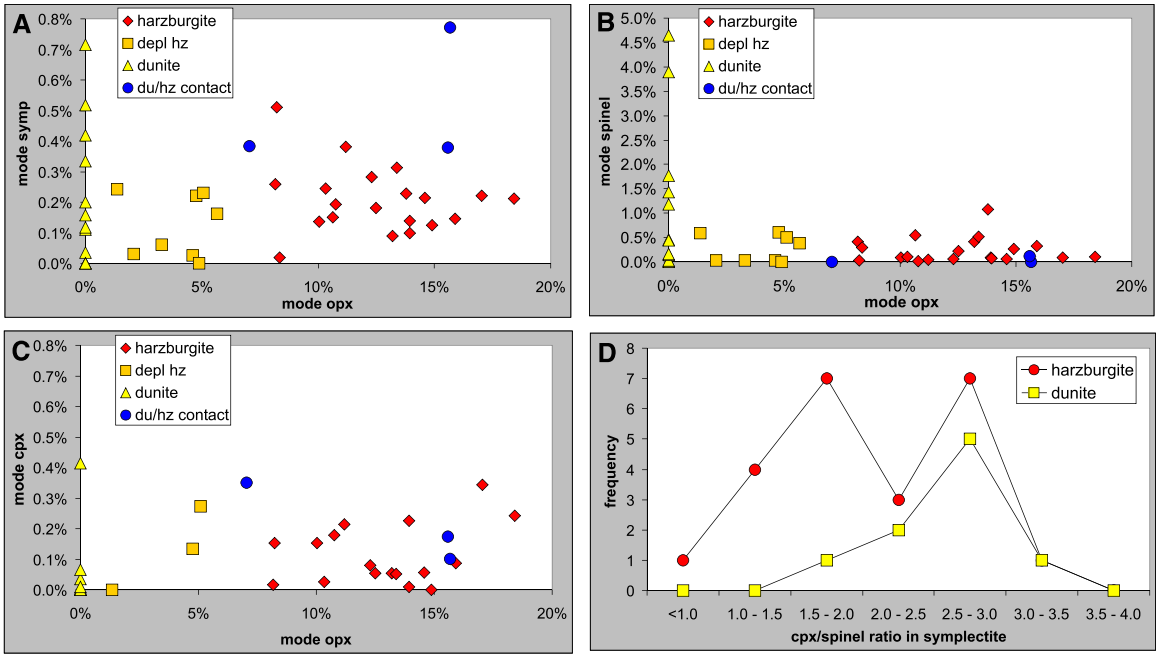

Figure 5. (a–c) Modes of opx, cpx, spinel, and symplectites and (d) ratio of modes in symplectites. (a) Symplectites tend to be more abundant in samples from the contact harzburgite to dunite. In dunites they are highly variable. (b) Spinels are locally very abundant in dunites. In opx-depleted harzburgites their mode corresponds to that of harzburgites. Samples from the dunite-harzburgite contact might have below average spinel modes. (c) Mode of cpx is below 0.4%, with no preference for any lithology. (d) Modal ratio of cpx to spinel in symplectites tends to be between 1.5 and 3. For Figure 5d, there is naturally a bias by assigning grains to being either a spinel with some cpx or a symplectite.

[*Aharonov et al.*, 1995; *Kelemen et al.*, 1995a, 1995b]). This model, if correct, would suggest a regional background percolation of a disequilibrium melt through the peridotite. Equation (1a) as applied to Site 1274A peridotites could thus be modified as

$$\mathrm{W\ melt1} + \mathrm{X\ opx} + \mathrm{Y\ cpx} + \mathrm{Z\ Al-spinel} + = \mathrm{A\ olivine} + \mathrm{B\ Cr-spinel} + \mathrm{C\ melt2} \quad (1b)$$

where X and Y in this case are the modal proportions of opx and cpx in the solid reactant, unlike in (1a) where the proportions of opx and cpx entering the melt are controlled by the stoichiometry of the melting reaction. As in (1a), Z and B depend on bulk composition, and A and C depend on pressure, but in addition W < C.

[24] *Seyler et al.* [2007] arrived at a similar interpretation, i.e., opx was replaced by secondary olivine. The result is relict opx surrounded by secondary olivine, either through a melting reaction or a percolating disequilibrium melt. *Seyler et al.* [2007] also observe olivine inclusions in spinel. They interpret the inclusions as relict olivine left behind after larger olivine was dissolved by Si-rich melts as derived by opx resorption.

5.2. Group 2: Rims or Coronas of Cpx on Opx (Figures 6 and 7)

[25] Cpx rims with variable thickness (μm to >100 μm range) are present between rounded opx and the olivine matrix but also between opx grains (Figures 6a–6f). They are never seen to be deformed or recrystallized, and thus postdate deformation. They are most abundant in samples from the immediate vicinity of dunites, but they have been observed to some extent in all thin sections of harzburgite from Hole 1274A available to us. If it is accepted that dunites carry a higher melt flux than the host rocks [e.g., *Kelemen et al.*, 1997], the higher abundance of cpx adjacent to dunites suggests that the rims of cpx represent the products of a reaction with melt or a direct crystallization product from melt. The rounded nature of opx suggests that opx was unstable during this reaction. Three different chronologies are possible:

[26] 1. Replacive formation of cpx after opx, triggered by reaction with melt. Cpx could have

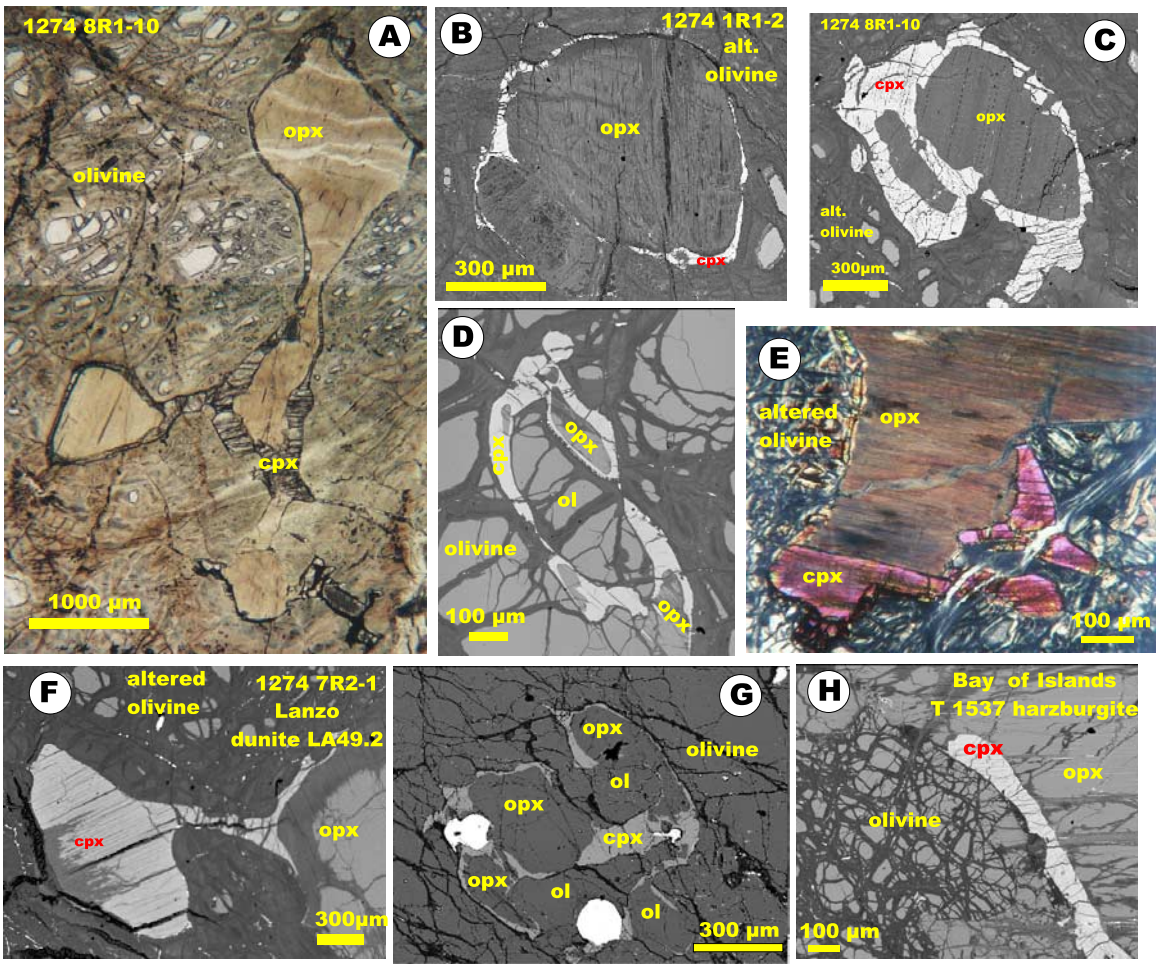

Figure 6. Backscattered electron images (Figures 6b–6d and 6f–6h) and microphoto in plane polarized light (Figure 6a) and with crossed nicols (Figure 6e) of Group 2 microstructures. Cpx rims are developed in variable thickness between the olivine matrix and opx grains. Samples are from Site 1274 as well as Lanzo Massif (Figure 6g) and the Bay of Islands Ophiolite (Figure 6h). The two pictures in Figures 6b and 6c demonstrate how conceivably two opx grains are progressively replaced by cpx along their rim and mutual grain boundaries. Larger cpx in Figure 6f might be a fully replaced former opx (see Figure 7 for model). In Figure 6h it appears that cpx completes the outline of a former opx grain, suggesting replacement. Note how the thickness of cpx varies along some rims.

formed from opx on the inside and could have either dissolved again at the outside or grew in thickness as progressively more opx was converted to cpx. In this model, cpx rims should largely mimic the original outline of opx, so the rounded nature of opx is not readily explained. This is a single stage model.

[27] 2. A two stage model whereby corrosion to form rounded opx is followed by replacive formation of cpx after opx. The reason for the switch in the reaction regime could have been a change in external physical conditions.

[28] 3. Another two stage model could be corrosion of opx by melt followed by direct precipitation of cpx from melt. Again, we would call for a change in external physical conditions to explain the change from opx dissolution to cpx crystallization.

[29] We know of no clear argument in favor of or against any one of these models. Some observations suggest, however, that cpx is probably replacive in most cases: (1) locally, cpx appears to "complete" the outline of a regular opx grain, i.e., it could be replacive (Figures 6e and 6h); (2) commonly, opx and cpx cleavage traces are parallel (Figure 6e), either indicating epitactic

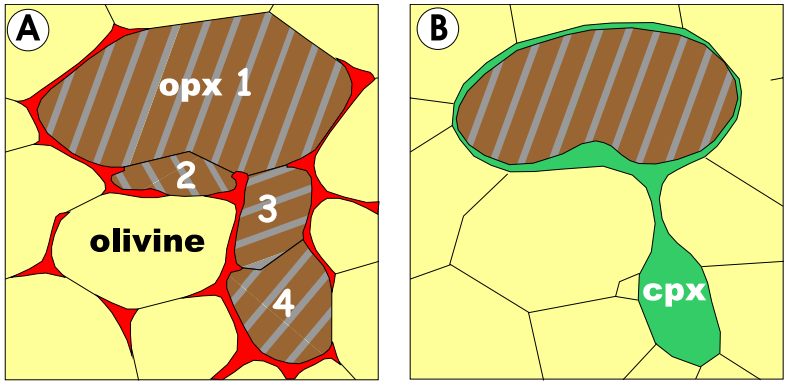

Figure 7. Model explaining formation of large cpx grains and generation of isolated opx grains from what was originally (Figure 7a) a multigrain opx cluster. Cpx in Figure 7b is thought to form transiently by reaction between melt (red) and opx, but to be ultimately resorbed into the melt unless the reaction is halted by temperature or time. Specifically, from Figure 7a to Figure 7b, opx grain 4 was transformed to cpx, opx grain 1 was partially resorbed, and thin selvages of cpx are all that is left of opx grains 2 and 3. All melt was extracted.

growth or again replacement; (3) comparing Figures 6b and 6c, a good case could be made that opx clusters are progressively consumed by cpx rims, with cpx growing as opx shrinks; and (4) another feature is that cpx rims may extend as interstitial films into the olivine matrix and then widen again into a massive cpx grain (Figure 6f). Would such interstitial/massive cpx be a magmatic precipitate? Perhaps, but another solution is that the entire volume now filled with cpx was once opx and that the massive cpx grain is a fully replaced opx grain (Figure 7). For example, in 7R2-2, smallest relics of opx are completely surrounded by cpx, suggesting that given more time, opx would have been completely replaced by cpx (Figure 6d).

[30] Very similar occurrences of cpx rims on opx are common in dunites from the Lanzo South Massif (Figure 6g). Again, cpx rims are most wide-spread in the contact zone between dunites and host rocks or in dunitic rocks which contain relict opx. Another example is given from a Bay of Islands Ophiolite harzburgite (Figure 6h). In this latter case, note that cpx fills an indentation in the outline of opx (supporting a replacement origin). The preferred reaction for formation of cpx rims and locally also cpx grains is thus

$$\text{opx} + \text{melt1} = \text{replacive cpx} + (?)\ \text{olivine} + \text{relict opx} + \text{melt2} \quad (2)$$

[31] The reason to argue for additional generation of olivine is that locally, as in Figures 6g, 8b, and 8c, olivine is observed between opx and its cpx rim or is located inside the cpx (Figure 8a). Perhaps in reaction (2), excess Fe and Mg from conversion of opx to cpx is deposited in olivine.

[32] Many dunites, both from Site 1274A and in the Lanzo South Massif (observations from Monte Arpone, Madonna della Bassa and Monte Musine) have very little to no cpx at all, whereas the contact zone between dunite and harzburgite commonly has cpx rims on opx (at Monte Musine in Lanzo, a variably thick harzburgitic selvage occurs between dunite and plagioclase lherzolite). Using the concept that dunites grow wider with time [e.g., *Suhr*, 1999], a contact zone will become a dunite at a later time. If the required assumptions are correct, this means that cpx which formed at the expense of opx in the contact zone (where we observe that it is commonly present) may dissolve again in dunite to account for the scarcity of cpx in many dunites.

[33] The chemical reason for reaction (2) is the well-known fact that melt saturated in olivine at higher pressure is undersatured in it at lower pressure [*O'Hara*, 1968; *Kelemen et al.*, 1995a]. Thus a Si-undersatured melt, carried within dunites to maintain disequilibrium [*Kelemen et al.*, 1995b], can react with host harzburgites and dissolve opx. The dissolution of opx, particularly when coupled with olivine precipitation, must have locally increased the Cr and Si concentration of the melt. *Liu and O'Neill* [2004] have shown that this will lower the activity of Al in the melt and this in turn will stabilize cpx. This can also be inferred by making the appropriate changes in the melt composition at near-liquidus concentrations in thermodynamic modeling software (e.g., A. E. Boudreau, Pele,

v.5.00, 2003; freeware available from http://www.env.duke.edu/eos/). It should be noted that a continuous layer of cpx on opx implies that the whole surface of a grain boundary, and not only triple-grain junctions, was able to react with melt during the available time. In summary, it seems likely that cpx was stabilized as a result of the reaction of melt with opx.

[34] *Seyler et al.* [2007] include evidence from base metal sulfides, and also report on samples with more abundant, large cpx grains. Their interpretation is that large cpx grains formed as early precipitates from a sulfide-rich melt, and subsequently were partially dissolved by percolating melts low in Al and Cr. As a result of this dissolution, the percolating melts reached cpx saturation and started to precipitate "cpx selvages which are left behind from melt."

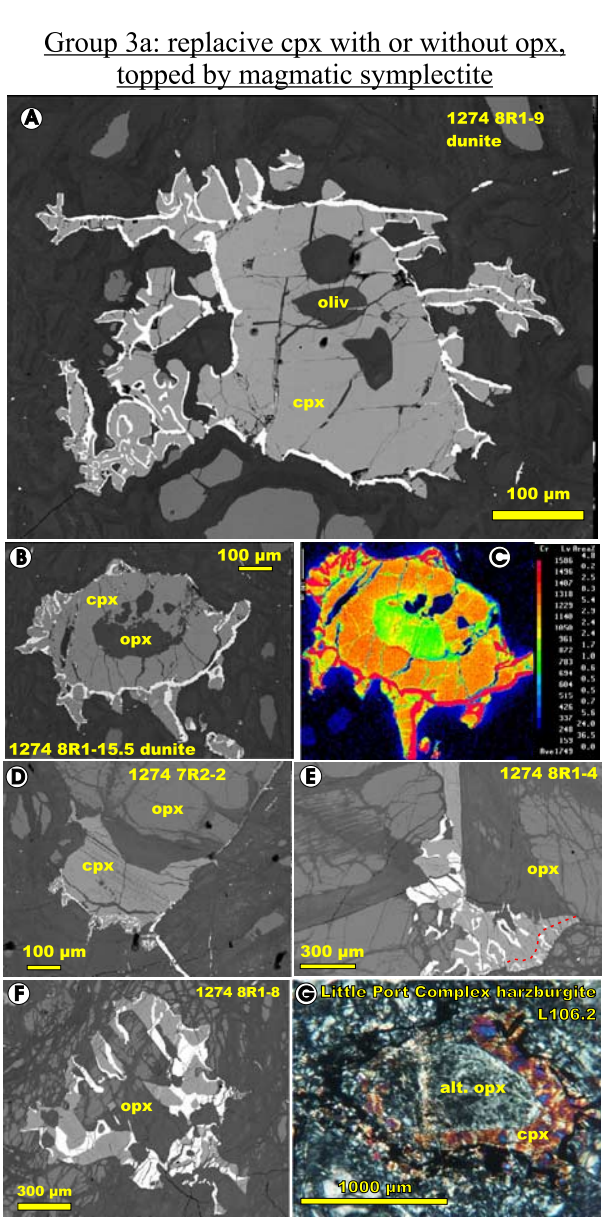

5.3. Group 3a: Cpx-Spinel Symplectite Rims (Figure 8)

[35] As mentioned above, the term symplectite is used here to describe a delicate, 10 μm or larger-scale intergrowth of spinel and pyroxene. Spinel-cpx symplectites occur in various microstructural locations, i.e., outside of cpx (Figures 8a–8d), outside of opx (Figures 8e and 8f), inside the olivine matrix (Figure 9; see section 5.4), and probably also outside of spinel (Figure 10a). More fine-grained symplectites occur at the outside of coarser symplectites (Figure 8e), suggesting that they are later and perhaps less modified by grain growth. The ratio of cpx to spinel is not distinctly different between more and less coarse intergrowths and an average value is about 5:2 (Figure 5d). Note the striking similarity of a symplectite from the Little Port Complex (Figure 8g, Bay of Islands Ophiolite) with the Site 1274A specimen in Figure 8b, i.e., rounded opx rimmed by a corona of cpx, in turn rimmed by cpx-spinel symplectite with irregular outlines toward olivine.

[36] Symplectites always share a face with olivine (Figure 8). The cpx-spinel symplectites never occur between a rim of cpx and its opx core or internal to cpx grains (Figure 11b). In all occurrences, a late origin is suggested by the peripheral location of the symplectite. This is corroborated by their highly irregular outline toward olivine which must post-

Figure 8. Backscattered electron images (Figures 8a, 8b, and 8d–8f), optical picture (Figure 8g), and Cr-distribution map (Figure 8c) of cpx-spinel symplectites placed either on top of cpx grains (Figures 8a–8d and 8g) or rimming opx (Figures 8e and 8f). Except for Figure 8g, all samples are from Site 1274. Outlines of symplectites toward the olivine matrix is highly irregular, best seen in Figures 8a and 8f. In Figure 8e a more delicate symplectite (SE corner, delineated by red dashed line) lies between the olivine matrix and a coarser symplectite, i.e., appears to be later. The coarser cpx-spinel intergrowth in Figure 8f might represent an annealed, formerly more delicate symplectite. Nonsymplectic cpx grains as in Group 2 may contain olivine inclusions (Figure 8a), form a corona on opx (Figures 8b, 8c, and 8g), or partially rim opx (Figures 8d and 8e). Interfaces between cpx and opx tend to be smooth, except for Figure 8f. In Figure 8c the Cr distribution of the grain shown in Figure 8b is given. Note that the core of the grain is a serpentinized opx with much higher Cr concentration than the olivine matrix.

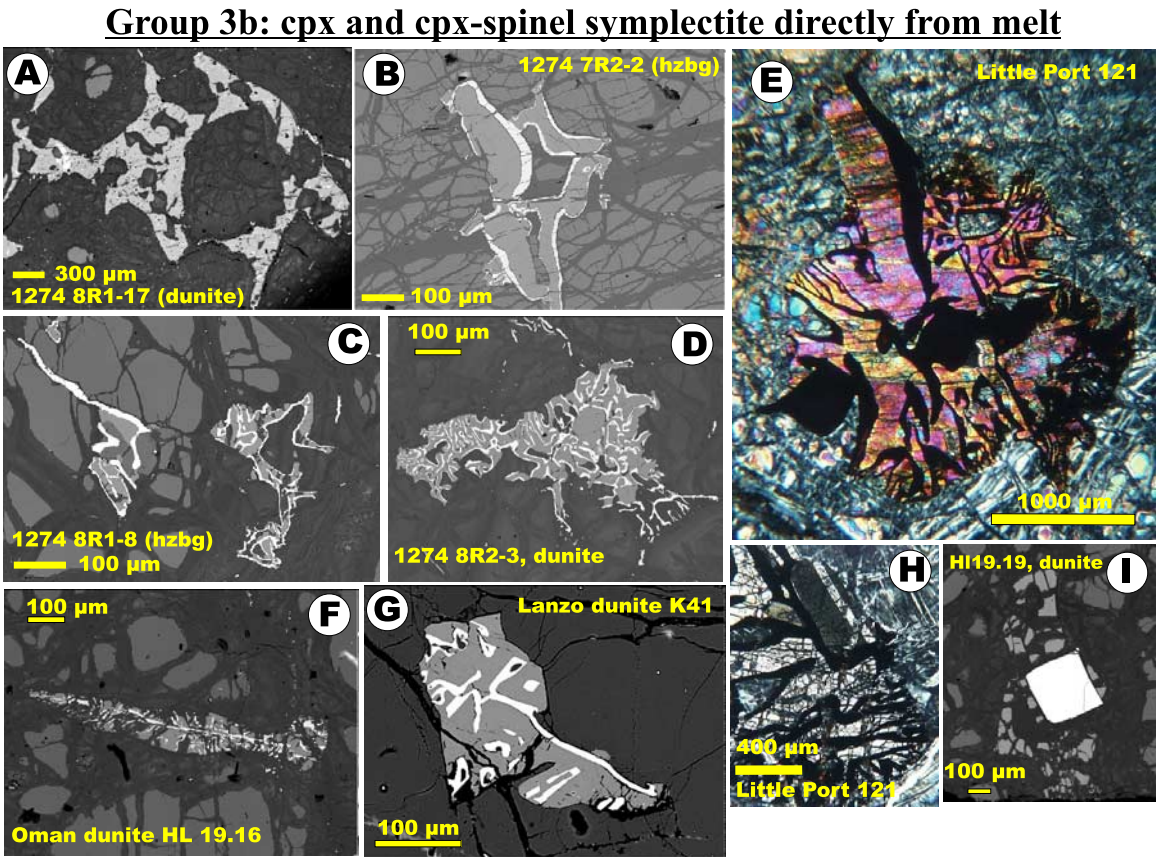

Figure 9. Backscattered electron images (except Figures 9e and 9h: optical images) of cpx and cpx-spinel symplectites occurring within the olivine matrix. Locations are Site 1274 (Figures 9a–9d), Monte Arpone in the Lanzo Massif (Figure 9g), Little Port Complex in the Bay of Islands Ophiolite (Figures 9e and 9h), and Haylayn Massif in the Oman Ophiolite (Figures 9f and 9i). Note coalescence of spinel septa toward the center in Figure 9e, perhaps indicating annealing. In Figure 9h a magmatic growth twin of cpx suggests a direct precipitation of cpx from melt. Occurrence of interstitial cpx-spinel in Figure 9i may represent a former symplectite as in Figures 9f and 9g, now annealed.

date plastic deformation and annealing. The origin of these symplectites is puzzling.

[37] Could the symplectites be an exsolution feature? In this case, the pre-exsolution pyroxene could be calculated as a recombination of cpx and spinel with a ratio of ~5:2. With typical compositional data from both minerals, this cpx would have had ~12 wt% Cr_2O_3. This is much too high for any realistic cpx. Exsolution features should also have a geometric spinel arrangement. Finally it would not be clear why only some grains, not others, have spinel exsolutions. Could the symplectites alternatively form in situ from chromium residual to pyroxene dissolution? This model, as attractive as it might seem, is unlikely because symplectites also are present within the olivine matrix and within dunites where there is no preserved evidence for the presence of opx. One would thus have to argue that symplectites in the olivine matrix represent a location where opx has just disappeared, or that symplectites represent a microstructurally stable feature, even after opx dissolution. Particularly for the case of dunites, where ongoing melt percolation is thought to occur, the long-term preservation of a delicate symplectite appears unlikely, because the symplectites represent a strong surface disequilibrium.

[38] Symplectites are a common occurrence during metamorphic reactions. Vermicular intergrowth of phases suggests limited diffusion for critical components, low nucleation rates, and a simultaneous growth of participating phases [*Vernon*, 2004, p. 242ff]. Symplectites are a reaction product from precursor phases typically still preserved next to the symplectites [*Vernon*, 2004]. In our occurrences, olivine is always in contact with the symplectites, suggesting that olivine is one of the reaction partners. Since "lobes of symplectites projecting

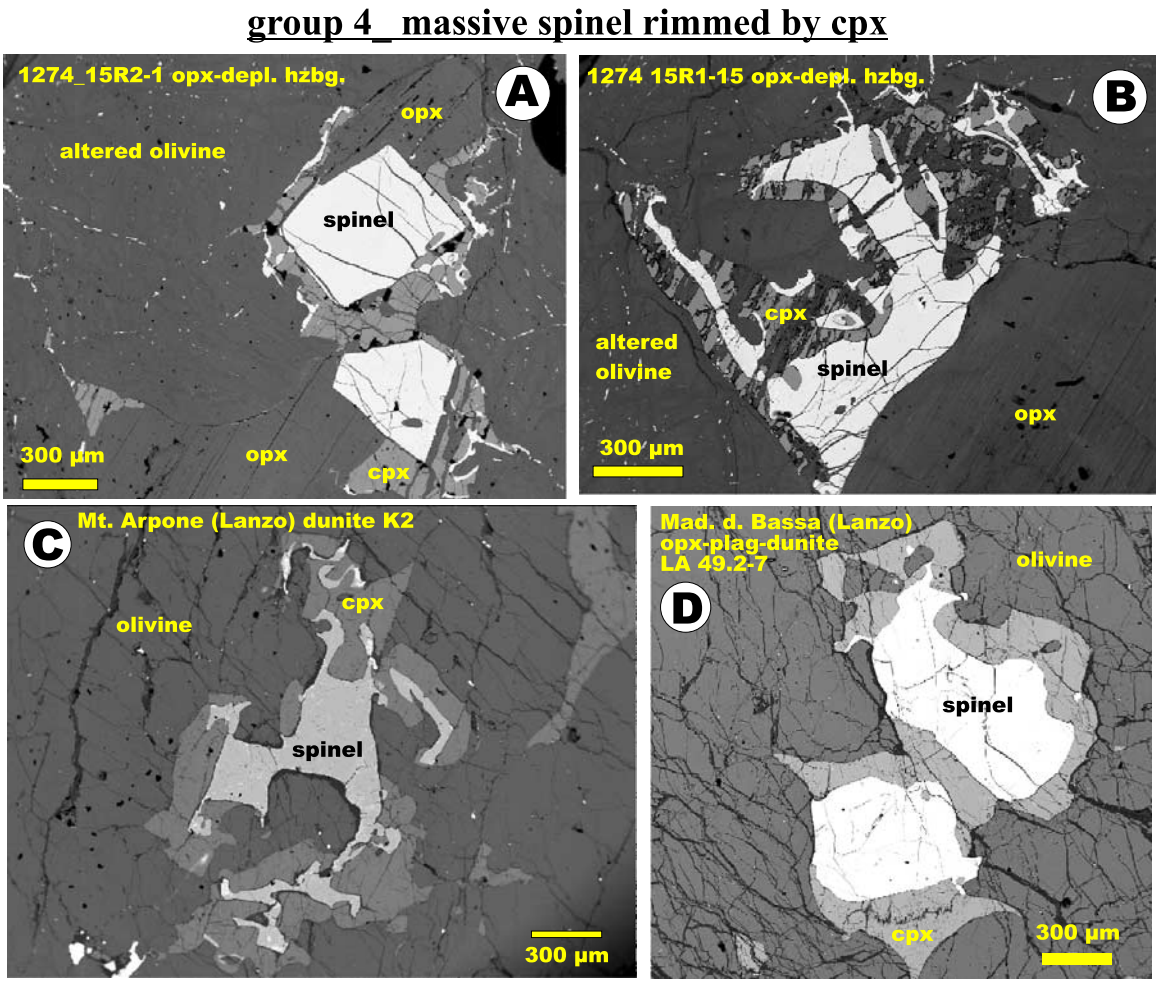

Figure 10. A group of microstructures with massive spinel being rimmed by cpx from (a and b) Site 1274 and (c and d) the Lanzo Massif. Possibly, it represents annealed spinel-cpx symplectites. However, their spinel/cpx ratio is larger than for typical symplectites. In all examples, (relict) opx either is still present in the same slide or, as in Figure 10d, is present in adjacent samples.

into the host phase indicate dissolution of the host phase" [*Vernon*, 2004, p. 244], the involvement, and dissolution, of olivine is supported. However, since symplectites grow on either olivine, cpx, opx, and probably other symplectites, the second reaction partner appears to be unimportant. Given the vast difference between the composition of these different phases, this makes little sense. Symplectites are most abundant near dunites, and dunites are likely former melt channels. Thus melt appears the probable second reaction partner, as in

$$\text{olivine} + \text{melt 1} = \text{cpx} - \text{spinel symplectite} \ (+\text{melt2}) \quad (3)$$

[39] Why would this reaction happen? After all, so far olivine precipitation, not resorption was postulated. All evidence, i.e., microstructural position at the outside of grains, lobate outline of symplectites suggesting a lack of strain, large surfaces suggesting limiting diffusion, indicate a late, relatively low temperature formation. The abundance at the dunite-host contact suggests some influence of the dissolution of opx. Thus we propose that melt migrating at a late stage through the peridotite network was (over)saturated in Cr from dissolution of opx. This melt thus precipitated spinel upon minor cooling. In turn this caused a slight increase in SiO_2 in the residual melt, which might have caused the postulated dissolution of olivine. The new porosity generated by olivine dissolution may have opened pathways for more melt. A high concentration in Cr and Si also lowers the activity of Al which was shown to increase the stability of cpx [*Liu and O'Neill*, 2004] and trigger cpx precipitation. Thus the relatively constant ratio of spinel to cpx may reflect this feedback.

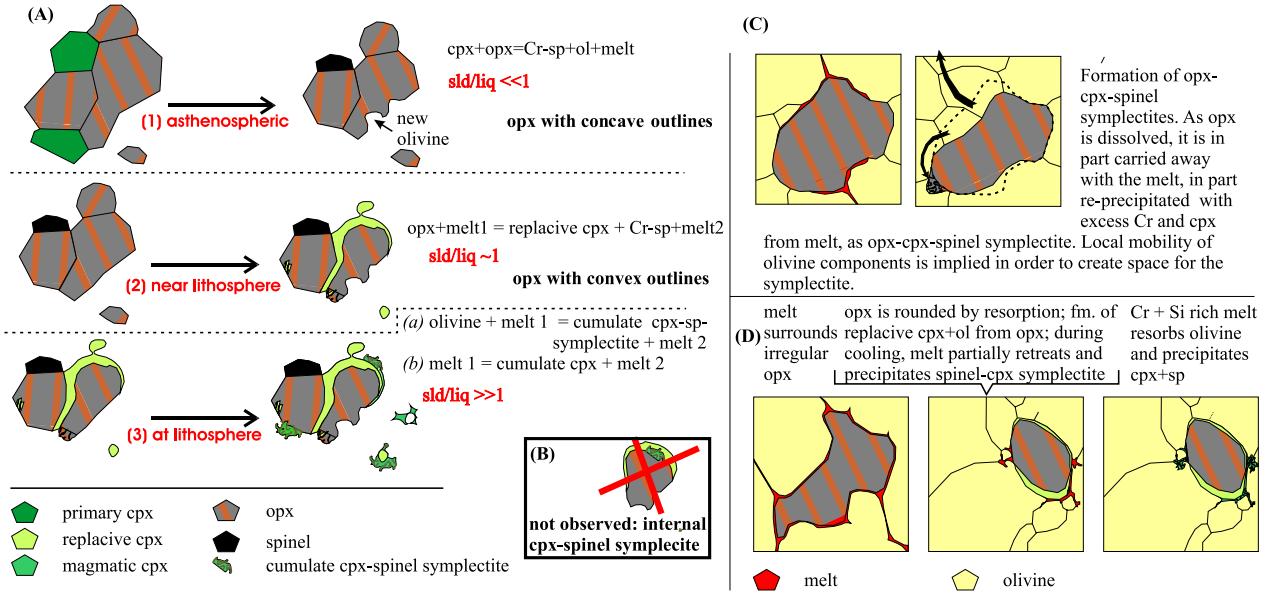

Figure 11. Simplified synthesis of the microstructural models; sld/liq refers to the ratio of melt consumed to melt generated during the reaction. (a) Formation of groups 1, 2, and 3. (b) A chronology with symplectites internal to cpx-rims; this has not been observed. (c) Model for the formation of opx-spinel symplectites with minor cpx, presumably occurring during stage 2 of Figure 11a. Melt causing the reaction is shown. (d) Model for the formation of groups 2 and 3; compared to Figure 11a, we show here additionally the melt causing the reaction.

[40] A problem is whether the combined effect of spinel precipitation and olivine dissolution would not decrease the activity of Cr and Si to the extent that cpx precipitation should stop. Notable in this context is that the symplectites are not spinel-opx, i.e., silica-activity was apparently too low to stabilize opx (but see section 5.5, opx-cpx-spinel symplectites). Why would symplectites not form all the time, i.e., why are cpx-spinel symplectites a late feature? Perhaps, only at a late, lower-temperature stage, the solubility and diffusivity of Cr and other components was very limited, resulting in formation of intimate intergrowths instead of more isolated, spatially separate crystals of spinel and cpx.

[41] If the above inferences are correct the question arises whether, in a given location, all symplectites formed in a single event or via a multistage process? Two constraints argue against a single stage process, i.e., formation from melt present in the intergranular network at any single time.

[42] The median of the modal abundance of symplectitic grains in harzburgites is 0.20 vol%. In dunites where the symplectite mode is more variable, the mean proportion of symplectites is 0.24 vol%. With a 5:2 volume ratio of cpx/spinel and averaged concentrations of Cr_2O_3 in cpx (1.20 wt%) and spinel (39.5 wt-%), the amount of Cr_2O_3 stored in symplectites in harzburgites is 0.024 wt%. The equilibrium concentration of Cr_2O_3 in basaltic melt at 1.1GPa and 1360 ± 20°C was recently determined by *Liu and O'Neill* [2004] as

$$[Cr_2O_3] = 0.009Cr\#_{sp} - 0.00096[K_2O]Cr\#_{sp}$$

where $Cr\#_{sp}$ refers to the molar Cr/(Cr + Al) ratio in the equilibrium spinel in the solid and $[K_2O]$ is the concentration of K_2O in the melt. For our conditions (low K_2O and Cr# 46 mol%), the solubility of Cr_2O_3 would be 0.41 wt%. This is much higher than the concentration of Cr_2O_3 of ~0.1 wt% typically observed in "primitive" MORBs, probably because, as *Liu and O'Neill* [2004] suggest, "primitive" MORB has actually fractionated some spinel. Retaining the high value of 0.41 wt% Cr_2O_3 in the melt, a minimum of 5.9 wt% of melt is needed to generate the typical modal proportion of symplectite in harzburgite by direct precipitation from the melt. (7.2 wt% melt in dunites). Lower Cr-solubilities would require higher proportions of melt. Even the minimum amount of melt required seems high as an instantaneous melt fraction ("porosity") in peridotite, so that symplectite formation was probably continuous during porous flow of melt through harzburgite. A second independent argument is that the presence of several generations of symplectites (more delicate outside of less delicate ones) suggests an ongoing process as opposed to a single event.

[43] *Seyler et al.* [2007] interpret the symplectites (their S2-generation) as a cotectic precipitate from a melt. We believe in the slightly more complex, but broadly similar explanation as outlined above.

5.4. Group 3b: Interstitial Magmatic Cpx and Cpx-Spinel Symplectite (Figure 9)

[44] If the above interpretation of symplectites is correct, a Cr-saturated melt and olivine is all that would be needed to make a symplectite. Symplectites should thus also occur within the olivine matrix and dunites, irrespective of the presence of opx or cpx, though dissolution of opx would certainly help to attain Cr-saturation. Indeed, symplectites have been observed, with the typical irregular outline and proportion, within the olivine matrix of both dunite and harzburgites (Figure 9). Locally, there is a central, rather massive cpx or spinel, the origin of which is not clear (Figures 9d and 9e). In Site 1274A dunites, interstitial cpx is also present, with most cpx being spinel-free, but some crystals being symplectic with spinel. Similar symplectites have also been observed in other peridotites, particularly Lanzo (Figure 9g), the Little Port Complex of the Bay of Islands Ophiolite (Figures 9e and 9h), and in an Oman dunite from the Haylayn Massif (Figure 9f). In the Little Port peridotites there is evidence for simple growth twins of cpx within the symplectite (Figure 9h), strongly suggesting a magmatic origin for cpx. Irregular outlines could again suggest olivine dissolution. Figure 9i may show an annealed, interstitial symplectite with a reduction in surface area of the spinel-cpx interfaces.

5.5. Symplectites Gradational From Opx-Spinel to Cpx-Spinel (Figures 4c–4e)

[45] A complicating observation in Hole 1274A peridotites is the occurrence of spinel-opx symplectites with minor amounts of cpx (Figures 4c, 4d, and 4e). Near the margin to the olivine matrix, the opx-spinel symplectites tend to change toward a cpx-spinel composition. The vermicular shaped spinels are continuous from opx to cpx-symplectites. A preferred occurrence of the symplectites near the tips of unequant opx grains seems typical, as already observed by *Seyler et al.* [2007]. A location outside of any cpx-rim or corona was never observed and deformation structures are not obvious.

[46] If we follow the lines of reasoning in the above interpretations, the cpx-spinel symplectite at the rim could be magmatic with some olivine dissolution (i.e., Figure 8), whereas the opx-spinel symplectite bears a resemblance to Figures 4a and 4b, i.e., have a residual signature acquired in the presence of a percolating melt.

[47] The textural similarity to cpx-symplectites, and the observed transition from opx to cpx symplectites at the rim, suggest that the opx-symplectites with minor cpx form in a kinetically similar way as the cpx-symplectites, i.e., mainly by precipitation from melt. The position near tips of elongate opx-grains may reflect local stress variations. Since a preferred position of these tips in a geometric reference frame was not observed, even on the scale of a thin section, the stress conditions would have to be very local, i.e., on a grain to grain scale. Our suggestion (Figure 11c) is that opx dissolution occurred in the presence of a melt followed by melt extraction (as for Group 1), but locally associated with oversaturation of the melt in opx-spinel and minor cpx, these phases reprecipitating near the tips of opx grains.

[48] For this to occur, we probably need some olivine redistribution from the site of opx-spinel precipitation to opx solution. Chronologically, the gradation of opx-symplectites into cpx symplectites (Figure 4d) suggests a formation just prior to the stage of cpx-symplectites. The chronology relative to corona-type cpx rims is not clear. Note that a residual nature of opx-spinel symplectites was suggested by *Leblanc et al.* [1980], who observed them in the vicinity of dunites.

[49] Opx symplectite with minor cpx were also described by *Seyler et al.* [2007] and classified as "S1." They assigned a higher-temperature origin to them than to the cpx-spinel symplectites. They are interpreted as "recrystallized opx parcels cemented by spinel and minor cpx, resulting from a melt which reacted with opx, then precipitated spinel and cpx." It thus appears that *Seyler et al.* [2007] prefer an in situ formation of the opx-cpx-symplectites, but to a first order, our interpretations are probably similar.

5.6. Group 4: Massive Spinel Rimmed by Cpx (Figure 10)

[50] A final observation refers mainly to the opx-depleted harzburgites, as they occur in cores 209-1274A-15R and -16R. Here, massive, locally euhedral spinel is rimmed by cpx, this association being partly encased in opx-grains (Figures 10a and 10b). The drastically reduced abundance of opx compared to regular harzburgites plus the lobate

shapes of opx crystals are evidence for opx having an origin as a relict.

[51] The problems of integrating this "group 4" with the other groups are as follows: (1) In the opx dunites, cpx is rimming spinel, i.e., spinel is apparently earlier than cpx, whereas in the spinel-cpx symplectite of group 3, cpx and spinel were considered contemporaneous. (2) Neither spinel nor cpx form a clear rim on opx. Instead, opx partly surrounds spinel and cpx (opx surrounding spinel is, however, typical of the inferred partial melting texture described as group 1). Locally, however, textures with cpx rimming opx, are present. (3) Chemically, some opx-depleted harzburgites are distinctly different from the rest of the peridotites, i.e., they are less depleted in incompatible trace elements (Figure 3) and significantly enriched in Cr_2O_3 in cpx and spinel compared to all other peridotites (Figures 2 and 3). (4) The opx-depleted harzburgites show no sharply defined contacts with other lithologies, unlike sharp harzburgite-dunite boundaries; instead, they form a diffuse zone with opx-depleted harzburgites grading into dunite [*Kelemen et al.*, 2004]. (5) Compared to the ratio cpx to spinel in the symplectites from harzburgites and dunites of ~5:2, this ratio is much smaller (i.e., more spinel relative to cpx) in the opx-depleted harzburgites.

[52] Similar textures to those observed in samples from 1274A-15R and -16R have been encountered in the Lanzo Massif (Figures 10c and 10d), locally with interstitial spinel extending into the cpx rim from a massive spinel core (Figure 10c). In Lanzo, opx tends to be physically separated from cpx-spinel but still be present in the same thin section. All occurrences shown in Figure 10, for both ODP Hole 1274A samples and non-1274A locations, tend to be in opx dunites or just internal to dunite-host contacts, so the presence of opx (again) appears to have been a factor. A virtually identical occurrence was described in the transition from harzburgite to dunite in New Caledonia, the difference being that in New Caledonia, opx, not cpx occurs [*Leblanc et al.*, 1980].

[53] A tentative interpretation is that opx in these textures is residual and that cpx-spinel represents a severely annealed symplectite of Group 3. The key is thought to be microstructural annealing which occurred during reaction between melt and host. The envisioned environment is one of slow melt-rock reaction coupled with high melt content, as would be realized where melts approach stagnation at a percolation boundary along the thermal boundary layer [e.g., *Sparks and Parmentier*, 1991]. The result would be saturation of melt with opx because supply with fresh, reactive melt was limited. In such an environment, reactions would inherently be slow relative to microstructural annealing, the latter being enhanced by the high melt content. This could explain the large, massive, locally euhedral spinel grains. Support for this model comes from geochemistry: the opx-depleted harzburgites have the highest Cr# in spinel (up to 56 mol% compared to 45 to 50 mol% in most samples, Figure 2) and the highest Cr2O3 contents in cpx (1.6 to 1.7 wt% compared to 1.2 to 1.3 wt% elsewhere), i.e., they were in equilibrium with a Cr-rich melt, the Cr being probably liberated during the conversion of opx to olivine. Further support for this hypothesis is provided by the diffuse occurrence of the opx-depleted harzburgites as opposed to the sharp dunite-harzburgite contacts normally seen in ophiolites (and the dunite at 41 mbsf in Hole 1274A). Obviously, the feedback loop between reaction and melt percolation operative for migrating melts [e.g., *Kelemen et al.*, 1995a] was disabled, perhaps due to melt stagnation. Why the cpx/spinel ratio is lowered compared to Group 3 is not readily apparent. Perhaps ambient temperatures were slightly higher.

6. Sequence of Events

[54] Given our preferred explanations for the microstructural features in peridotites from Site 1274, we now synthesize them into an evolutionary model. The microstructural observations suggest a chronology of events with symplectic rims being later than cpx-rims, and cpx rims being later than coarse spinel associated with opx (Figure 11). As an overriding framework, we use an asthenospheric upwelling regime which encountered the base of the mantle lithosphere (Figure 12). This is considered a likely environment for igneous processes at Site 1274 [*Kelemen et al.*, 2004]. Note that the following sequence of events can be fit into system where progressively less melt is generated and more melt is consumed.

6.1. Highest-Temperature Conditions (Asthenospheric)

[55] Melting reactions (1a) and (1b) are assigned to asthenospheric decompression melting. Typical features are a high temperature, well-recovered olivine microstructure, the near absence of cpx grains due to consumption during melting, and a redistribution of Cr as seen in localized opx-spinel

clusters. A large amount of melt must have been generated, on the basis of the chemical and mineralogical depletion. At a later stage, there appears to be more melting related to infiltration of a disequilibrium melt from depth, as seen in the highly lobate opx-outlines (reaction (1b)). These lobate textures must have formed at a late stage of the deformation history as their lack of preferred shape orientation suggests that there has been no subsequent overprint by deformation and attainment of low-energy surface equilibration. For this regime, we infer

$$\text{volume melt generated} > \text{volume melt consumed}$$

[56] Highly unradiogenic Os-data [*Harvey et al.*, 2006] suggest that the substantial melting event for Site 1274A peridotites took place billions of years ago, unrelated to the current spreading center. Could concave, irregular outlines in opx grains of the peridotites survive billions of years? Probably not. More likely, these formed in the later, current convective stage of the Mid-Atlantic spreading regime.

6.2. Subasthenospheric Temperatures Near the Conductive Lithosphere

[57] In our view, cpx rims on rounded opx reflect conversion of opx to cpx. Formation of cpx is not associated with lower pressure partial melting, so a melting-only origin is ruled out. We believe that replacement of opx by cpx occurred near the base of the conductive lithosphere. In order for melt generation to proceed, a source of heat must have been present, i.e., concomitant dissolution and precipitation of phases from melt, balanced by the heat of fusion [e.g., *Kelemen et al.*, 1990]. In terms of melt balance, this regime is thought to be less productive than in the adiabatic decompression, or asthenospheric, regime because of the inferred replacive origin of cpx. There is no trace of plastic deformation associated with these microstructures, so that plastic flow of the peridotite under a spreading ridge must have ceased during this stage. Instead, because these rocks are now exposed on the seafloor, uplift of rigid tectonic blocks between localized shear zones and faults must have occurred. This means that a small amount of decompression melting may still have occurred during this stage. The inferred melt balance is

$$\text{volume melt generated} \cong \text{volume melt consumed}$$

6.3. Moderately High Temperatures at Base of Conductive Lithosphere

[58] Symplectite formation from melt, plus minor olivine resorption, is assigned to a regime with significant cooling at the base of the conductive lithosphere. Melt is now mainly consumed such that

$$\text{volume melt generated} < \text{volume melt consumed}$$

[59] Minor olivine may be consumed at this stage. Microstructures with high surface energies remain preserved, so it appears unlikely that the peridotites resided at high temperatures for an extended period of time. Instead, cooling and efficient freezing of small scale textural relationships is indicated.

6.4. Stagnating Conditions

[60] Group 4 microstructures are tentatively put into an environment where drainage of melt was poor, i.e., near a permeability barrier, probably again at the base of the conductive lithosphere (Figure 12).

7. Is There a Relation Between the Geodynamic History of the Peridotites and the Observed Microstructures?

[61] As already mentioned, the tectonic setting of Site 1274 is complex. Os-isotopes support a model in which some depletion is ancient. Did Site 1274 peridotites undergo any melting at all in the current Atlantic mantle upwelling/decompression regime? As argued above, pristine features like lobate opx-outlines, undeformed cpx-rims, and intricate spinel-pyroxene symplectites require a recent melt generation process. We prefer the following scenario. Ancient depletion of harzburgites in an old convection cycle was followed in recent times by renewed decompression melting and melt infiltration, causing the undeformed, melt-related features. Because these features are most pronounced next to dunites, the dunites might have been the loci of percolation also for the late migrating melts. Is the dunite at 41 mbsf also an ancient melt channel rejuvenated in recent times? This is difficult to answer with the available data. In any case, it seems clear that in the recent convective regime, it carried some melt, products of which are preserved as undeformed microstructures within the dunite and particularly at its contact to the host harzburgites.

[62] The peculiar aspect of this study is that a similar scenario (early melting, later melt infiltration) was previously postulated for the two other localities which were cited here as examples of microstructural analogues to Hole 1274A perido-

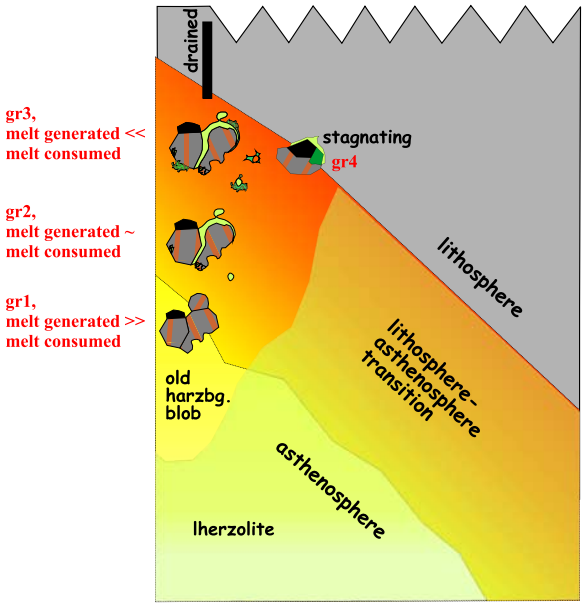

Figure 12. Placement of microstructural groups within the subridge environment. Note the suspected occurrence within an anciently depleted harzburgitic blob of poorly constrained extent. As depth of base of lithosphere, 15–20 km has been suggested [*Kelemen et al.*, 2004].

tites. For the Lanzo Massif, the most recent interpretations argue for a pre-alpine depletion event, perhaps even in a subcontinental mantle environment, with much later melt infiltration during opening of the Ligurian Ocean [*Müntener et al.*, 2004; *Piccardo et al.*, 2004]. For the Little Port Complex, we know that its age is 17 Ma older than that of the adjacent Bay of Islands Complex [*Kurth et al.*, 1998]. Probably, the Little Port, arc-type lithosphere was rifted to accommodate an oceanic spreading ridge that formed the Bay of Islands Complex, this event being linked to melt and fluid infiltration into the older arc lithosphere [*Suhr and Edwards*, 2000]. To our knowledge, similar pristine and widespread examples of cpx rims and spinel-cpx symplectites have not been reported from occurrences in intermediate to fast spreading ophiolites though local occurrences surely will be present and are expected to be present. After all, the mechanisms described are far from unique.

[63] So what could be the link between the tectonopetrologic scenario described and the state of preservation and abundance of cpx rims on opx and delicate symplectites? Our suggestion is that microstructures related to infiltration are best preserved when the peridotites are frozen into a steep position under a spreading center, i.e., slow spreading ridges with isotherms dipping steeply away from the spreading center. During viscous corner flow typical for fast spreading ridges with shallowly dipping isotherms, any such microstructures are likely to be overprinted by plastic strain or be annealed at high temperature. While freezing may well be effective for subhorizontal flow away from a spreading center, the large shear strains accumulated during the corner flow event [*Blackman et al.*, 2002] might be the limiting factor for preservation of pristine melting and reaction textures.

[64] The relation of these textures to the ancient depletion seems more peculiar at first. An explanation might be a link to melt connectivity. Depleted peridotites rich in olivine and poor in pyroxenes are predicted to have high permeability at a given melt fraction, compared to peridotites rich in pyroxene [*Toramaru and Fujii*, 1986; *Zhu and Hirth*, 2003]. Typical slow spreading conditions, with a deep asthenosphere-lithosphere boundary, will lead to termination of melting before high degrees of depletion are reached. If melting starts with a fertile peridotite, a lherzolitic residue with relatively low permeability will still be present at base of the lithosphere [*Langmuir et al.*, 1992]. On the other hand, if the upwelling peridotite had been previously depleted, a (more permeable) harzburgitic residue is a likely end-product of upwelling even under slow spreading conditions.

[65] Thus the conditions that produce and preserve the pristine hypersolidus microstructures observed in samples from Site 1274 probably include (1) slow spreading, with a deep transition from adiabatic to conductively cooled mantle and steeply dipping isotherms; (2) a previously depleted source entering the melting regime which is olivine-rich, with high permeability to melt; and (3) a source to generate melt.

[66] Concerning this latter point, it seems possible that the previously depleted source yielded some additional melt in the current Atlantic upwelling regime. Note that the 15°20′ fracture zone is clearly not amagmatic. About 30% gabbroic intrusions into peridotite were sampled by drilling on Leg 209. This is also the proportion of gabbro to peridotite recovered in dredging and submersible sampling in the region (summaries of *Kelemen et al.* [2004]). Alternatively, we must consider that Hole 1274A depleted peridotites represent a small volume of highly depleted material with more fertile material present deeper in the mantle (Figure 12) [cf. *Seyler et al.*, 2003]. Melts from such a source may also have percolated in small quantities

through the previously depleted, permeable residue exposed at Site 1274A.

[67] The only piece of independent evidence that melts exotic to Site 1274A peridotites have actually interacted with these peridotites comes from the opx-depleted peridotites at cores 15R and 16R. These peridotites include cpx which is less depleted in HREE, Ti, and Na than cpx in the rest of the peridotites (Figure 3). Melts in equilibrium with these opx-depleted harzburgites are still very different from MORBs from the region, but they give us a hint that more fertile sources might be present at depth.

8. Conclusions

[68] We describe a distinctive set of microstructures in harzburgites, opx-depleted harzburgites, and dunites [cf. *Seyler et al.*, 2007]. These microstructures are not unique to Site 1274 peridotites. Aspects of these microstructures are probably present in peridotites worldwide. However, they are rarely preserved in such a pristine condition, with a clear chronological order and in such abundance. It is suggested that the observed microstructures represent a temporal progression of melting, melt percolation, and reaction during cooling, as the peridotite progressively intersected the lithosphere-asthenosphere boundary during upwelling. Reactions can be formulated to describe the textural relationships that indicate a progressively increasing ratio of melt consumed to melt generated, as one would expect for the proposed thermal evolution. The excellent development of the microstructures may be due to the combination of slow spreading and the presence of a previously depleted, permeable peridotite. This last conclusion is derived mainly by comparison of observations from Hole 1274A samples to textures in other peridotites where such microstructures are also preserved, and where such a combination of factors might also have been present.

Acknowledgments

[69] The first author wants to extend his special thanks to the 209 Scientific Party, including Eiichi Kikawa and Jay Miller, for permitting postcruise work on samples from Hole 1274A, even though circumstances prevented him from participating in the cruise. We also thank Walter Hale for help during postcruise sampling at the Bremen Core Repository. Supporting reviews by Monique Seyler and Shoji Arai as well as comments and efficient editorial handling by Vincent Salters improved the manuscript. Financial support of the first author by the Deutsche Forschungsgemeinschaft (DFG) is gratefully acknowledged.

References

Aharonov, E., J. A. Whitehead, B. Kelemen, and M. Spiegelman (1995), Channeling instability of upwelling melt in the mantle, *J. Geophys. Res.*, *100*, 20,433–20,450.

Asimov, D. (1999), A model that reconciles major- and trace-element data from abyssal peridotites, *Earth Planet. Sci. Lett.*, *169*, 303–319.

Blackman, D. K., H.-R. Wenk, and J. M. Kendall (2002), Seismic anisotropy of the upper mantle: 1. Factors that affect mineral texture and effective elastic properties, *Geochem. Geophys. Geosyst.*, *3*(9), 8601, doi:10.1029/2001GC000248.

Bonatti, E., A. Peyve, P. Kepezhinskas, N. Kurentsova, M. Seyler, S. Skolotney, and G. Udintsev (1992), Upper mantle heterogeneity below the Mid-Atlantic Ridge, 0°–15°N, *J. Geophys. Res.*, *97*, 4461–4476.

Cannat, M., D. Sauter, V. Mendel, E. Ruellan, K. Okino, J. Escartin, V. Combier, and M. Baala (2006), Modes of seafloor generation at a melt-poor ultraslow spreading ridge, *Geology*, *34*(7), 605–608.

Dick, H. J. B., J. Lin, and H. Schouten (2003), An ultraslow spreading class of ocean ridge, *Nature*, *426*, 408–412.

Dosso, L., H. Bougault, and J.-L. Joron (1993), Geochemical morphology of the north Mid-Atlantic Ridge, 10°–24°N: Trace element-isotope complementarity, *Earth Planet. Sci. Lett.*, *120*, 443–462.

Fujiwara, T., J. Lin, T. Matsumoto, P. B. Kelemen, B. E. Tucholke, and J. F. Casey (2003), Crustal evolution of the Mid-Atlantic Ridge near the Fifteen-Twenty Fracture Zone in the last 5 Ma, *Geochem. Geophys. Geosyst.*, *4*(3), 1024, doi:10.1029/2002GC000364.

Harvey, J., A. Gannoun, K. W. Burton, N. W. Rogers, O. Alard, and I. J. Parkinson (2006), Ancient melt extraction from the oceanic upper mantle revealed by Re-Os isotopes in abyssal peridotites from the Mid-Atlantic ridge, *Earth Planet. Sci. Lett.*, *244*, 606–621.

Hellebrand, E., J. E. Snow, H. J. B. Dick, and A. W. Hofmann (2001), Coupled major and trace elements as indicators of the extent of melting in mid-ocean ridge peridotites, *Nature*, *410*, 677–681.

Hellebrand, E., J. E. Snow, P. Hoppe, and A. W. Hofmann (2002), Garnet-field melting and late-stage refertilization in 'residual' abyssal peridotites from the Central Indian Ridge, *J. Petrol.*, *43*, 2305–2338.

Jaques, A. L., and D. H. Green (1980), Anhydrous melting of peridotite at 0–15 Kb pressure and the genesis of tholeiitic basalts, *Contrib. Mineral. Petrol.*, *73*, 287–310.

Johnson, K. T., H. J. B. Dick, and N. Shimizu (1990), Melting in the oceanic upper mantle: An ion microprobe study of diopsides in abyssal peridotites, *J. Geophys. Res.*, *95*, 2661–2678.

Kelemen, P. B., D. B. Joyce, J. D. Webster, and J. R. Holloway (1990), Reaction between ultramafic rock and fractionating basaltic magma II. Experimental investigation of reaction between olivine tholeiite and harzburgite at 1150–1050°C and 5 kb, *J. Petrol.*, *31*, 99–134.

Kelemen, P. B., J. A. Whitehead, E. Aharonov, and K. A. Jordahl (1995a), Experiments on flow focusing in soluble porous media, with applications to melt extraction from the mantle, *J. Geophys. Res.*, *100*, 475–496.

Kelemen, P. B., N. Shimizu, and V. J. M. Salters (1995b), Extraction of MORB from the mantle by focussed flow of melt in dunite channels, *Nature*, *375*, 747–753.

Kelemen, P. B., G. Hirth, N. Shimizu, M. Spiegelman, and H. J. B. Dick (1997), A review of melt migration processes in the adiabatically upwelling mantle beneath oceanic spreading ridges, *Philos. Trans. R. Soc. London, Ser. A*, *355*, 283–318.

Kelemen, P. B., E. Kikawa, J. Baldauf, and J. Miller (2002), Leg 209 scientific prospectus: Drilling mantle peridotite along the Mid-Atlantic Ridge from 14° to 16°, 47 pp., Ocean Drill. Program, College Station, Tex. (Available at http://www-odp.tamu.edu/publications/prosp/209_prs/209prosp.pdf)

Kelemen, P. B., et al. (2004), Leg 209 summary, *Proc. Ocean Drill. Program Initial Reports*, *209*, 83–212.

Kurth, M., A. Sassen, G. Suhr, and K. Mezger (1998), Precise ages and isotopic constraints for the Lewis Hills (Bay of Islands Ophiolite): Preservation of an arc-spreading ridge intersection, *Geology*, *26*, 1127–1130.

Langmuir, C. H., E. M. Klein, and T. Plank (1992), Petrological systematics of mid-ocean ridge basalts: Constraints on melt generation beneath ocean ridges, in *Mantle Flow and Melt Generation at Mid-ocean Ridges*, *Geophys. Monogr. Ser.*, vol. 71, edited by J. Phipps Morgan, D. K. Blackman, and J. M. Sinton, pp. 183–280, AGU, Washington, D. C.

Leblanc, M., C. Dupuy, D. Cassard, J. Moutte, A. Nicolas, A. Prinzhoffer, M. Rabinovitch, and P. Routhier (1980), Essai sur la genèse des corps podiformes de chromitite dans les péridotites ophiolitiques de Nouvelle-Calédonie et de Méditerranée orientale, in *Ophiolites: Proceedings of the International Ophiolite Symposium, Nicosia, Cyprus*, *1979*, edited by A. Panayiotou, pp. 691–701, Geol. Surv. Dep., Nicosia, Cyprus.

Liang, Y., and D. Elthon (1990), Evidence from chromium abundances in mantle rocks for extraction of picrite and komatiite melts, *Nature*, *343*, 551–553.

Liu, X., and H. O'Neill (2004), The effects of Cr_2O_3 on the partial melting of spinel lherzolite in the system CaO-MgO-Al_2O_3–SiO_2–Cr_2O_3 at 1.1 GPa, *J. Petrol.*, *45*, 2261–2286.

Macdonald, K. (2005), Mid ocean ridges, in *Encyclopedia of Geology*, edited by R. C. Selley, L. R. Cocks, and I. R. Plimer, pp. 372–387, Elsevier, Amsterdam.

MELT Seismic Team (1998), Imaging the deep seismic structure beneath a mid-ocean ridge: The MELT experiment, *Science*, *280*, 1215–1218.

Michael, P., et al. (2003), Magmatic and amagmatic seafloor generation at the ultraslow-spreading Gakkel Ridge, Arctic Ocean, *Nature*, *423*, 956–961.

Müntener, O., T. Pettke, L. Desmurs, M. Meier, and U. Schaltegger (2004), Refertilization of mantle peridotite in embryonic ocean basins: Trace element and Nd isotopic evidence and implications for crust-mantle relationships, *Earth Planet. Sci. Lett.*, *221*, 293–308.

Nicolas, A. (1989), *Structures of Ophiolites and Dynamics of Oceanic Lithosphere*, 367 pp., Kluwer, Dordrecht, Netherlands.

Nicolas, A., and F. Boudier (1995), Mapping oceanic ridge segments in Oman ophiolite, *J. Geophys. Res.*, *100*(B4), 6179–6198.

O'Hara, M. J. (1968), Are ocean floor basalts primary magma, *Nature*, *220*, 683–686.

Parker, R. L., and D. W. Oldenburg (1973), Thermal model of ocean ridges, *Nature*, *242*, 137–139.

Piccardo, G. B., O. Müntener, A. Zanetti, and T. Pettke (2004), Ophiolitic peridotites of the Alpine-Apennine System: Mantle processes and geodynamic relevance, *Int. Geol. Rev.*, *40*(11), 1119–1159.

Reid, I., and H. R. Jackson (1981), Oceanic spreading rates and crustal thickness, *Mar. Geophys. Res.*, *5*, 165–172.

Seyler, M., M. Cannat, and C. Mével (2003), Evidence for major-element heterogeneity in the mantle source of abyssal peridotites from the Southwest Indian Ridge (52° to 68°E), *Geochem. Geophys. Geosyst.*, *4*(2), 9101, doi:10.1029/2002GC000305.

Seyler, M., J. P. Lorand, H. J. B. Dick, and M. Drouin (2007), Pervasive melt percolation reactions in ultra-depleted refractory harzburgites at the Mid-Atlantic Ridge, 15°2′N: ODP Hole 1274A, *Contrib. Mineral. Petrol.*, *153*, 303–319.

Sleep, N. H. (1975), Formation of oceanic crust: Some thermal constraints, *J. Geophys. Res.*, *80*, 4037–4042.

Sparks, D. W., and E. M. Parmentier (1991), Melt extraction from the mantle beneath spreading centers, *Earth Planet. Sci. Lett.*, *105*, 368–377.

Suhr, G. (1999), Significance of upper mantle hosted duite bodies for melt migration and extraction under oceanic spreading centres: Inferences from reactive transport modeling, *J. Petrol.*, *40*, 575–599.

Suhr, G., and S. J. Edwards (2000), Contrasting mantle sequences exposed in the Lewis Hills Massif: Evidence for the early, arc-related history of the Bay of Islands Ophiolite, in *Ophiolites and Oceanic Crust: New Insights From Field Studies and Ocean Drilling Program*, edited by Y. Dilek et al., *Spec. Pap. Geol. Soc. Am.*, *349*, 433–442.

Toramaru, A., and N. Fujii (1986), Connectivity of melt phase in a partially molten peridotite, *J. Geophys. Res.*, *91*(B9), 9239–9252.

Turcotte, D. L., and J. Phipps Morgan (1992), The physics of magma migration and mantle flow beneath a mid-ocean ridge, in *Mantle Flow and Melt Generation at Mid-ocean Ridges*, *Geophys. Monogr. Ser.*, vol. 71, edited by J. Phipps Morgan, D. K. Blackman, and J. M. Sinton, pp. 155–182, AGU, Washington, D. C.

Vernon, R. H. (2004), *A Practical Guide to Rock Microstructure*, 594 pp., Cambridge Univ. Press, Cambridge, U. K.

Walter, M. J. (2003), Melt extraction and compositional variability in mantle lithosphere, in *Treatise on Geochemistry*, edited by H. D. Holland and K. K. Turekian, pp. 363–394, Elsevier, Amsterdam.

Workman, R. K., and S. R. Hart (2005), Major and trace element composition of the depleted MORB mantle (DMM), *Earth Planet. Sci. Lett.*, *231*, 53–72.

Zhu, W. L., and G. Hirth (2003), A network model for permeability in partially molten rocks, *Earth Planet. Sci. Lett.*, *212*, 407–416.